Surface & Coatings Technology 448 (2022) 128893

Contents lists available at ScienceDirect

Surface & Coatings Technology

journal homepage: www.elsevier.com/locate/surfcoat

Study on nano-graphitic carbon coating on Si mold insert for precision glass molding

Lin Zhang *, Jiwang Yan

Department of Mechanical Engineering, Faculty of Science and Technology, Keio University, Yokohama 223-8522, Japan

ARTICLE INFO

Keywords:
Precision glass molding
Nano-graphitic carbon coating
Surface characterization
Si mold insert
micro-optics components

ABSTRACT

Precision glass molding is an efficient and promising technique for large-volume micro-optical manufacturing. Even though significant progress in precision glass molding has been achieved on the anti-adhesive coating, technical challenges and barriers still exist towards tailoring the coating layer to ensure durability and long-term processing consistency in numerous molding cycles. This manuscript presents a novel molding technique utilizing micro-patterned Si mold inserts coated with a newly developed nano-graphitic carbon coating as an isolation layer in high-precision glass molding. The coating is prepared by atmospheric pressure chemical vapor deposition (APCVD), in which the liquid benzene and silicone rubber are used as the carbon source and silicon oxycarbide (SiOC) source, respectively. The nano-morphologies of the nano-graphitic carbon coating with different conditions are characterized and analyzed, illustrating notable differences in surface features with the addition of silicone rubber and various growth durations. In the demonstration, the nano-graphitic carbon-coated Si mold inserts exhibit unique properties, including anti-adhesive and hydrophobic at elevated temperatures. Two kinds of micro-patterned Si mold inserts, a micro-pillar matrix and a micro-lens array, generated by UV lithography and diamond turning, are utilized to demonstrate the feasibility of the anti-adhesive coating in precision glass molding. The obtained results indicate that the micro-optical features on the coated Si mold inserts are successfully transferred to glass substrates with high replication fidelity without notable signs of adhesion or contamination in repetitive molding cycles. This emerging technology makes Si an alternative mold material with low surface adhesion, enhances micro-optical machining efficiency, and replicates high-precision, low-cost micro-optics on large scales that were previously unavailable.

1. Introduction

Advanced optics with sophisticated micro-structures have inspired extensive applications and innovations in biomedical devices, telecommunication systems, and optical applications [1–3]. Recently, the massive use of micro-optics in optical devices can improve the optical properties or allow for compact dimensions, or a combination of these attractive features, which prompts a great demand for various micro-optics with high geometrical consistency, surface integrity, and machining efficiency [4]. Cost-effective manufacturing approaches to large-scale micro-optics have gained increasing attention in the industry. Among them, mechanical machining is more universal and deterministic. Even though some conventional mechanical techniques are popular in the mass production of large-aperture glass optics, these processes are no longer suitable for micro-optics with sophisticated and high-precision dimensions, such as Shack-Hartmann wavefront sensors, diffractive optical elements (DOE) and artificial bionic compound eyes [5]. Recently, single-point diamond turning and high-speed micro-milling are promising techniques for micro-optic fabrication with high-precision dimensions. However, it is likewise a challenge to generate such micro-optics on large scales with low cost due to certain inherent defects of these techniques, such as low machining efficiency and inevitable tool wear [6]. In addition, since most of the optical materials belong to the hard/soft-brittle material class, the machining-induced surface/subsurface defects significantly affect the optical performance of the final products [7].

Among various micro-optics fabrication techniques, precision glass molding (PGM) is an efficient and promising process for large-scale micro-optical manufacturing, which should be attributed to its simplicity in tools and operation process compared with other machining processes. More importantly, this technique is a near-net-shape manufacturing method capable of generating sophisticated

* Corresponding author.
E-mail address: zhanglin@keio.jp (L. Zhang).

https://doi.org/10.1016/j.surfcoat.2022.128893
Received 13 July 2022; Received in revised form 14 September 2022; Accepted 14 September 2022
Available online 20 September 2022

micro-structures on a large area of glass substrate at elevated temperatures [3,8]. As a replication process, regardless of material properties, such as soft/hard and brittle at ambient temperature, it significantly improves machining productivity and geometrical consistency compared with conventional mechanical processes. Generally, most of the micro-optics made by PGM can be directly employed in various optical devices without further processing, which has demonstrated great commercial success in a wide range of applications.

As a thermal forming process, PGM makes use of the unique characteristics of glass material at elevated temperatures to change the profile of glass substrates. For a typical PGM process, the tool assemblies and glass substrates are heated to the pre-determined molding temperature, which is generally slightly beyond the transition temperature (T_g) of the glass substrates, and subsequently squeezed into the desired shape with a constant molding force. Before releasing the molded glass optics from the mold insert, the temperature descends to the ambient temperature with a controlled cooling rate. Unfortunately, the interfacial adhesion at elevated temperature and thermal shrinkage after cooling results in glass/mold insert cracking or even failure, interrupting the process repetition and escalating the overall cost [9]. A new anti-adhesive coating technique, which can eliminate glass-mold insert interfacial adhesion at elevated temperature and reduce resistance coefficient, is critical to overcoming this issue in PGM.

Massive efforts have been devoted to achieving anti-adhesive coating material on mold inserts. These coatings can be classified into metallic coatings [10–15], ceramic coatings [16–19] and carbon-based coatings [5,20,21]. The metallic coatings generally utilize some rare and noble metals, such as Pt, Re, and Ir, because of their high chemical inertness at elevated temperatures, even up to 700 °C. For instance, Zhu et al. developed the monolayer of Re, Ir, and multilayers of Re/Ir on tungsten carbide cobalt (WC-Co) mold inserts to mitigate the interfacial sticking and attempt to extend the lifespan of the mold inserts [15]. Fischbach et al. investigated the Pt—Ir coating on WC-Co substrates in precision glass molding and the glass-to-mold sticking force at elevated temperatures [12]. However, such metallic coatings are considered an excessively expensive process, not only due to the high cost of the rare and noble metal but also the complicated coating process. In addition, the interfacial element diffusion and surface oxidation are potential threats to the metallic coating at elevated temperatures, leading to the collapse of the surface coating [22], which, in turn, drives more searches for alternative anti-adhesive coatings. Ceramic coatings, like silicon carbide (SiC), silicon nitride (Si_3N_4), and aluminum oxide (Al_2O_3), have been widely applied in precision glass molding with varying degrees of success [17,19]. For example, Zhang et al. adopted a newly developed α-Al_2O_3 multilayer coating by CVD on the binderless WC mold insert [16]. To enhance the interfacial adhesion, multilayer materials, including TiN, Ti(C, N), and Ti(C, O) from the bottom to the top, are deposited as transition interlayers, which make it difficult to keep the geometrical accuracy and compensate thermal deformation at elevated temperatures [22]. The superiorities of carbon-based coatings attract a large amount of attention from scientific and industrial communities due to their exceptional mechanical, electrical, and tribological properties, which can be tailored from super hard to soft and lubricant by adjusting the sp^3/sp^2 carbon hybridization ratio. Graphene is a newly developed carbon-based material consisting of single/multiple layers of atoms arranged in a two-dimensional (2D) honeycomb lattice nanostructure [23]. He and Li et al. utilized the carbide-bonded graphene coating as an anti-adhesive layer on mold inserts in visible band optical glass and infrared (IR) band chalcogenide glass molding [5,20]. Li et al. synthesized an amorphous carbon coating by magnetron sputtering on WC-8Co substrates and investigated the thermal stability and surface friction coefficient [24]. More experimental research on coating strength and oxidation at elevated temperatures is still needed before widespread applications [25]. The other important carbon-based coating material, diamond-like carbon (DLC), has been widely used in the plastic injection molding and hot-embossing process. Due to the graphitization above 450 °C, which completely changes the lattice structure of DLC, the surface integrity and strength seriously deteriorates, as well as the time-in-service. Thus, it is inappropriate to be employed in PGM when the molding temperature is above the tipping point of graphitization [26].

Carbon is one of the most stable elements under oxygen-free conditions, and carbon-based coatings generally illustrate excellent thermal conductivity that promotes heat transfer and temperature uniformity in precision glass molding. In this manuscript, we introduce a new technique that can be adopted to eliminate the adhesion between Si material and glass by using a nano-graphitic carbon coating, which also illustrates the unique advantages of low surface friction and high thermal conductivity. The building of a solid and homogeneous nano-graphitic carbon coating as a non-stick layer on a Si mold insert is conducted by atmospheric pressure chemical vapor deposition (APCVD). Silicon oxycarbide is deliberately utilized in the transition layer between the Si mold insert and the nano-graphitic carbon coating to enhance the adhesion strength. The process parameters are optimized through a series of experiments to obtain admirable surface smoothness by modulating the element contents and changing growth duration. The micro/nano-morphologies and surface roughness are further characterized and analyzed. Furthermore, the coated Si mold inserts with different micro-structures are demonstrated in precision glass molding. Notably, this newly developed coating enables the adoption of Si as the mold material, which most materials cannot match in terms of versatility of microscale fabrication, material durability and availability, for large-scale high-precision glass optics fabrication, and lead to a low-cost manufacturing approach.

2. Methodology and experiment

2.1. Atmospheric pressure chemical vapor deposition

Nano-graphitic carbon coating is deposited on polished and micro-patterned Si mold inserts by one-step APCVD. As illustrated in Fig. 1 (a), the Si mold insert with a dimension of 20 × 20 × 0.5 mm^3 and a piece of silicone rubber are pre-placed at the center of a quartz tube (Φ 45 mm × 600 mm). Anhydrous benzene in a glass bubbler with a purity of 99.9 % and high-temperature silicone rubber is utilized as the carbon and silicon sources, respectively. An inert gas, argon, is used as a protective gas to purge the residual air from the quartz tube with the initial

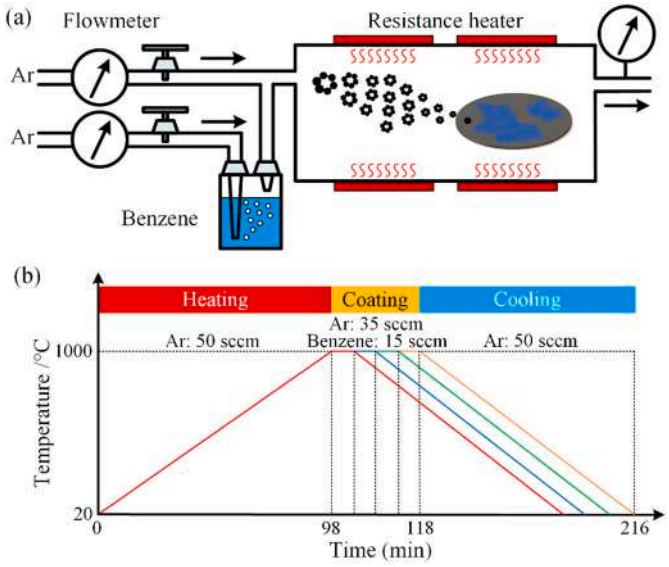

Fig. 1. (a) Schematic diagram of atmospheric pressure chemical vapor deposition setup for coating on Si mold inserts, and (b) variation of process parameters as a function of coating time.

flow rate of 60 standard cubic centimeters per minute (sccm) for 15 mins. Then, the flow rate is reduced to 50 sccm. After that, the temperature inside the quartz tube furnace rises to the pre-set coating temperature (1000 °C) under the protective gas at a constant heating rate of 10 °C/min, as illustrated in Fig. 1(b). Once the pre-set coating temperature is reached, anhydrous benzene is carried into the quartz tube by bubbling at a flow rate of 15 sccm, whereas the protective gas is tuned to 35 sccm to keep a constant total flow rate of 50 sccm. After holding at the growth temperature for several minutes, the carrier gas is turned off, and the protective gas flow rate is turned to 50 sccm. Finally, the temperature cools down naturally to the ambient temperature before the coated Si mold inserts are removed from the quartz tube. The duration that the pre-set coating temperature is held is defined as the growth duration, which might significantly influence the coating thickness and surface smoothness. The surface micro/nano-morphologies and some physical/chemical properties of the nano-graphitic carbon coating could be tuned by changing the growth durations or modifying the element contents. In this study, the growth durations are set at 5 mins, 10 mins, 15 mins, and 20 mins, and different amounts of high-temperature silicone rubber (0 g, 0.1 g, 0.3 g, and 0.5 g) are used to optimize the surface morphology.

After the coated Si wafer is cleaned with acetone and dried with nitrogen gas, a cross-sectional lamella of the nano-graphitic carbon-coated Si mold insert with a dimension of 20 × 10 × 1 μm^3 is extracted using a focused ion beam system (FIB, Quanta 3D FEG, FEI Company, USA). The preparation of the lamella can be divided into four steps. First, a layer of platinum (Pt) is deposited on the sample surface to protect the coating. Then, the focused ion beam creates pits all around the lamina with a high material removal rate, which usually takes several minutes. After cleaning the cross-sectional surfaces, a U-shape abrasion under and on the two sides of the lamella is conducted and left minor part to bridge the substrate. Finally, the lamella is bonded to a micro-manipulator by Pt deposition, and the bridge is cut off to transfer the lamella to a copper grid for further observation. The surface micro/nano-morphologies and the hierarchical structures of the cross-sectional lamella are examined using a field-emission scanning electron microscope (FE-SEM, MERLIN Compact, Carl Zeiss AG, Germany). The element compositions of the coating surface and the transition layer are analyzed by an energy dispersive X-ray spectrometer (EDX, Bruker AXS, Germany) coupled with the FE-SEM at an acceleration voltage of 5– 10 kV. Due to the excellent conductivity of the coating, the surface micro/nanoscale features can be directly observed without additional conductive coating on the sample surface. The surface three-dimensional (3D) micro/nano-morphologies for both the coated and uncoated Si mold inserts are obtained by a white-light interferometer (Zygo@ Nexview™ NX2, AMETEK Inc., USA) and an atomic force microscope (AFM, AFM5100N, Hitachi High-Technologies Corp., Japan). A laser micro Raman spectroscope (Renishaw Plc., UK) is used to analyze the microstructures of the nano-graphitic carbon coating with an excitation wavelength of 532 nm. In addition, the crystalline structure of the nano-graphitic carbon coating is also measured by an X-ray diffraction (XRD) instrument, D8 Advance (Bruker AXS, Germany). The chemical bonds of the nano-graphitic carbon coating are characterized by X-ray photoelectron spectroscopy (XPS, ESCALAB 250Xi, Thermo Fisher Scientific Inc., USA).

2.2. Micro-feature fabrication on Si wafer

Although some non-metallic materials, such as WC, glassy carbon, and nitride ceramics, are regarded as potential candidates for mold materials, most of them cannot catch up with the Si material in terms of micro/nanofabrication and material availability, which is suitable to serve as mold material [27]. Several mature processing techniques, such as standard ultraviolet (UV) lithography-based micro-machining and high-precision diamond turning machining, can be adopted in microstructure fabrication on Si material [28]. This study adopts two kinds of micro-structures, including a micro-pillar matrix and a micro-lens array, as mold inserts. For the micro-pillar matrix, contact UV lithography is adopted to pattern binary micro-structures on the Si wafer, followed by inductively coupled plasma reactive ion etching (ICP-RIE) [25]. As illustrated in Fig. 2(a), S1813 photoresist is initially spinning on the surface of a double-side polished Si wafer, which is further patterned by with 5 μm × 5 μm square matrix with a 5 μm gap via UV exposure. After a several-minute developing process, the Si wafer is sculpted with micro-patterns via dry etching by reactive CF_4 gas plasma at a flow rate of 20 sccm. Target etching depth (i.e., 450 nm) can be precisely achieved by adjusting the etching conditions (flow rate, power, and time). Finally, the residual photoresist is dissolved and cleaned by acetone bath and isopropyl alcohol (IPA). The micro-lens array, which consists of 58 spherical concave lenslets, has a hexagonal pattern in a circular region with a diameter of 2.5 mm. Each lenslet has an aperture diameter of 320 μm. The radius of curvature for each lenslet is 2.563 mm, resulting in an effective focal length of 4.746 mm for the K-PG375 glass. For the micro-lens array machining, it is directly fabricated on a Si wafer using a CNC ultra-precision lathe (Nanoform X, AMETEK Inc., USA), as shown in Fig. 2(b) [29]. A commercial natural single-crystal diamond tool with a round cutting nose of 1.0 mm, a rake angle of −30°, and a flank angle of 36°, is employed in slow tool servo (STS) diamond turning. To achieve uniform and good surface integrity, the rough and finishing cutting depths are set as 4.0 μm and 2.0 μm with a constant feed rate of 1 μm/rev. The obtained average surface roughness of the Si mold insert is about S_a 5 nm.

2.3. Precision glass molding

Several molding tests are carried out on a commercial compression molding apparatus GMP-211 (Toshiba Inc., Japan) to characterize the feasibility and effectiveness of the newly developed coating in repetitive molding cycles. Before the molding experiment, micro-patterned Si wafers and the cylinder-shaped glass substrate are shown in Fig. 3(a). Precision glass molding follows the typical four phases, including preparing, heating, pressing, and cooling, as shown in Fig. 3(b). Initially, the cylinder-shaped glass substrate is sandwiched between two Si mold inserts. Then, a protective gas, nitrogen, is used to prevent the molding assemblies from oxidation at elevated temperatures. A small gap (about 1 mm) is adjusted between the glass and the mold insert to ensure sufficient heat transfer in the heating phase. To eliminate any cracking and failure inside the glass substrate, the pre-set molding temperature is kept for several minutes to ensure that the glass substrate is heated up thoroughly before pressing. Then, a compression load is applied to the mold insert to squeeze the softened glass into the micro-patterns. After that, a slightly lower holding pressure is used in the cooling phase to compensate for thermal shrinkage and minimize the residual stress for high geometrical accuracy and optical quality. The molded glass is released from the mold insert when the temperature cools to ambient temperature through fast cooling.

2.4. Materials

The Si material used in the experiments is a double-side polished single-crystal Si wafer with a thickness of 500 μm. The micro features are generated on the (001) crystallographic plane. The diamond tool further divides the Si wafer into small pieces (20 × 20 × 0.5 mm^3). A specially formulated glass for precision glass molding, K-PG375 (Sumita Optical Glass Inc., Japan), is adopted with a softening temperature of 367 °C and molding temperature of 375 °C. Based on the size of the Si mold inserts, the glass preforms are polished into a cylindrical shape with a diameter of 8.0 mm and a height of 6.0 mm. In the durability tests, the other oxide glass P-SK57 (Schott Glass Inc., Germany) is adopted with a diameter of 10.0 mm and a height of 5.0 mm. The transition temperature is 493 °C, and the molding temperature is 550 °C based on previous research [30].

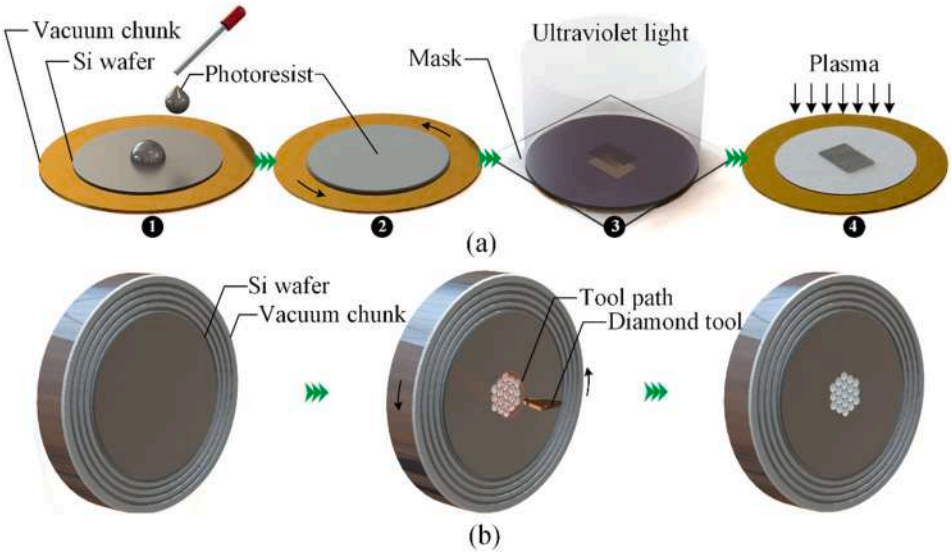

Fig. 2. Schematic diagrams of the micro-pattern fabrication processes, (a) contact UV photolithography, 1. dropping photoresist on a Si wafer; 2. spin-coating photoresist; 3. UV exposure; 4. plasma etching, and (b) single-point diamond turning of the micro-lens array on a Si wafer.

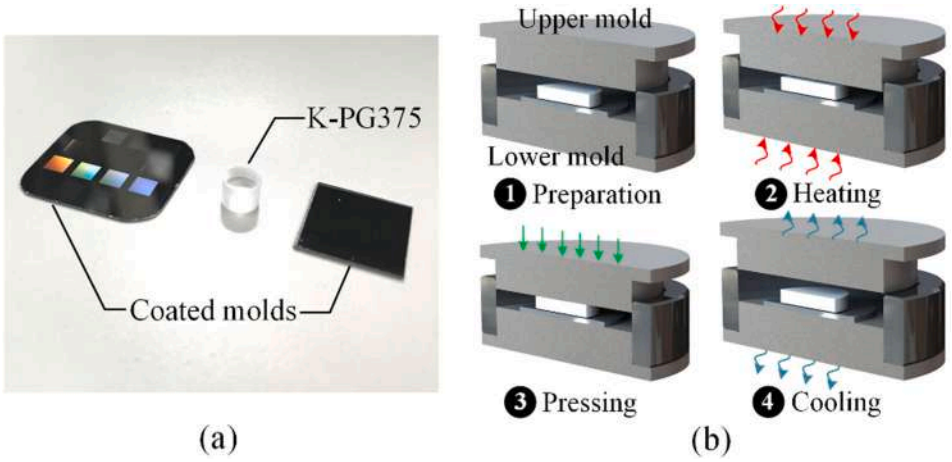

Fig. 3. (a) Photography of the coated Si mold inserts and a cylinder-shaped glass substrate, and (b) schematic diagrams of the PGM process, 1. preparation; 2. heating; 3. pressing; 4. cooling.

3. Results and discussion

3.1. Coating characterization

Before being utilized in molding experiments, the surface micro/nano-morphologies of the coated Si wafer should be characterized. Fig. 4 illustrates the SEM images of the nano-graphitic carbon coating with different amounts of silicone rubber as the modifying element in the APCVD process. The silicone rubber is used in the coating process with weights of 0 g, 0.1 g, 0.3 g, and 0.5 g. The growth duration (10 mins) and other conditions are the same. As the micro/nano-morphologies illustrated in Fig. 4, homogeneous nanoscale island-like domains covering the Si wafer without noticeable gaps are achieved, indicating the uniformity and consistency of the coating. Unlike the current metal-catalyzed graphene CVD coating on nickel or copper, which only deposits serval layers of graphene with poor adhesion to the substrates, the nano-graphitic carbon coating on Si wafer, consisting of nanoscale island-like domains, can directly attach to the Si mold insert with a remarkable enhancement of interfacial adhesion strength. According to the previous studies, the nanoscale island-like domains should be attributed to the narrow reaction window of the carbon growth on the Si material, much smaller than that on the metallic material, i.e., nickel and copper [31,32]. In addition, it is notable that due to the introduction of silicone rubber, the average size of the island-like domains decreases, and the surface profile becomes smoother because the nanoscale island-like domains are more efficient in covering the Si wafer with better homogeneity [27]. Compared with the fully covered Si wafers, in Fig. 4(c), some vacancies appear on the coated Si wafer. It should be attributed to the initial surface defects or dirt on the Si wafer, which inhibit the carbon growth on these positions.

Further analysis on the nano-graphitic carbon coating is conducted to investigate the effect of silicone rubber in the APCVD process to alter the nano features of the island-like domains. The nano features of the nano-graphitic carbon coating are obtained by statistical analysis of the island-like domains. For clearly distinguishing the boundaries between the adjacent domains, the back-scattered electron (BSE) images of the nano-graphitic carbon-coated Si wafers are obtained and utilized for further processing. The grey-scale images after post-processing based on the BSE images are shown in Fig. 5. From the obtained results in Fig. 5(a) to (d), the nanoscale island-like domains illustrate various characteristics of morphology and homogeneity. To gain an intuitive view of the differences, a statistical analysis on the size of the nanoscale island-like

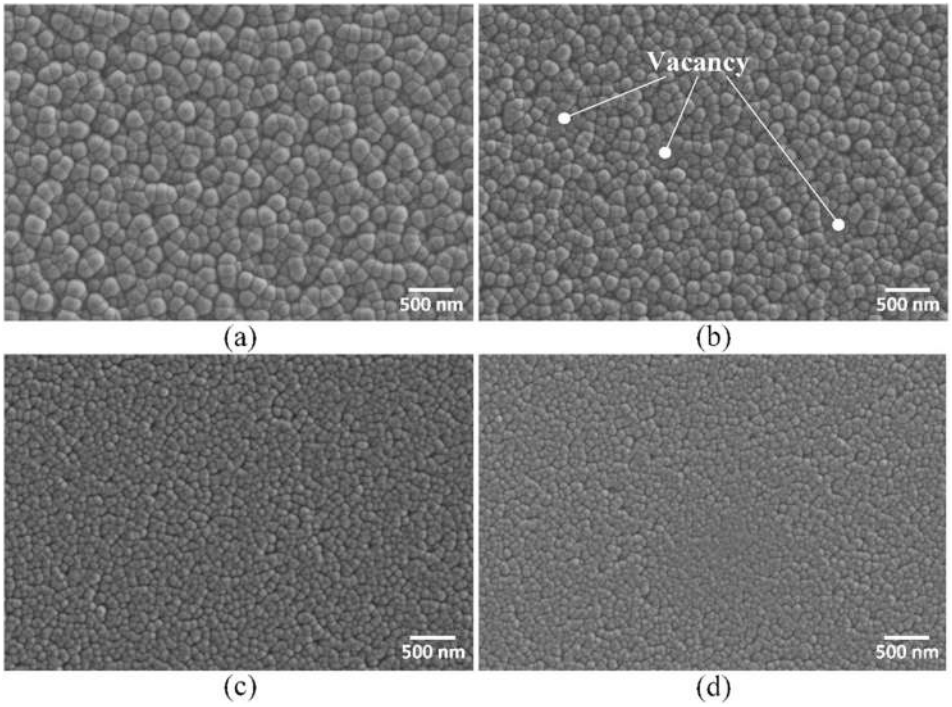

Fig. 4. SEM images of the nano-graphitic carbon coating grown with silicone rubber as the modifying element in the APCVD process, (a) 0 g, (b) 0.1 g, (c) 0.3 g, and (d) 0.5 g.

domains is conducted, and the corresponding results are illustrated in Fig. 5(e). For simplifying the study, the projected shape of the island-like domains is assumed to be a circle, and the discrete statistical results are in the normal distribution. From the results shown in Fig. 5(e), the discrete histograms and the corresponding fitted normal distribution curves clearly illustrate the differences in the average size and consistency. It is noticeable that with the introduction of silicone rubber in the APCVD process, the average diameter of the nanoscale island-like domains becomes smaller but has better homogeneity, which can also be supported by the characteristics shown in Fig. 4. The average value of the diameter and the statistical variance obtained from Fig. 5(e) are shown in Fig. 5(f). The average diameter of the island-like domains is 83.4 nm without silicone rubber, which is decreased to 65.3 nm, 50.7 nm, and 45.9 nm with the addition of 0.1 g, 0.3 g, and 0.5 g silicone rubber. The grain size variation should be attributed to the effect of atomic impurities, atomic rearrangement, and diffusion mobility in the nano-graphitic carbon coating growth [33].

Furthermore, the nano-morphologies of the carbon coating are achieved by AFM. Fig. 6(a) to (d) display the AFM micrographs of the nano-graphitic carbon coating grown with and without silicone rubber, and some local areas are enlarged and shown in Fig. 6(e) to (h). The AFM micrographs (Fig. 6(a) and (b)) of nano-graphitic carbon coating grown without and with a weight of 0.1 g silicone rubber illustrate a similar triangle-shaped layer. The shape of the carbon coating indicates the crystalline structure due to the orientation-dependent formation energy in CVD coating [34], which is also supported by Raman spectra shown in Fig. 7. Two high and sharp peaks, a D peak at 1357 cm^{-1} and a G peak at 1595 cm^{-1}, are typical characteristics of the existence of crystalline structures [35]. From the enlarged view of the 3D topography in Fig. 6 (e), the side lengths of the triangle layer are about 37.5 nm, 44.3 nm, and 49.7 nm. Whereas, in Fig. 6(f), even though the shape of the carbon coating is close to a triangle, the size becomes much smaller, and the profile is less irregular than that in Fig. 6(e), which is usually a combination of several smaller domains. Different from the nano-structures in the above, the growth behavior of carbon coating on single-crystal Si wafer with more amount of silicone rubber is distinct in terms of shape and size as shown in Fig. 6(c) and (d). The nano-morphologies of the carbon coating are no longer planar triangle-shaped layers but spherical clusters with an average diameter between 40 nm to 60 nm. It indicates carbon spherical clusters are more favorable than the planar triangle-shaped layers growth with more silicone rubber, which should be attributed to the modifying element affecting the growth process of nano-graphitic carbon coating in the APCVD process and leading to different nano-morphologies of the carbon coating [34]. The results suggest that silicone rubber plays a critical part in determining the nano-morphologies of the nano-graphitic carbon coating.

The lattice structures of the nano-graphitic carbon coating are further measured by the Raman spectroscope. From the results shown in Fig. 7, typical peaks of the graphitic network are observed on the nano-graphitic carbon-coated Si wafer, the D peak at 1357 cm^{-1} and the G peak at 1595 cm^{-1}, which are strong support for the presence of sp^3 and sp^2 carbon bonds in the graphitic networks [36]. Raman spectra of the nano-graphitic carbon coating indicate quite a sharp G peak, which is upshifted ~15 cm^{-1} by the compressive stress corresponding to a compressive stressed hexagonal cyclic sp^2 cluster structure. Meanwhile, the measured D band maximum at 1357 cm^{-1} shows a similar upshift as the G peak due to the compressive stress, which is close to the Ge_A peak (Graphene A-edges edge). Furthermore, the Raman spectra also indicate a broader left side D band corresponding to disordered rhombohedral and hexagonal chair diamond-like structures [37]. From the inset in Fig. 7, a visible shoulder appears primarily in the case with a large amount of silicone rubber. Compared with D and G band peaks, the intensity of the 2D band at 2714 cm^{-1} is relatively inconspicuous, indicating the presence of a large number of graphite layers. Besides the peaks of the nano-graphitic carbon coating, a minor peak is located near 521 cm^{-1}, which should be due to the single-crystal Si wafer beneath the coating layer. The coating process mixed the structures of graphite and diamond-like structures, combining hardness and lubrication properties, which is expected to be suitable for high-temperature applications.

From the features in the XRD spectra, as shown in Fig. 8, besides the characteristic peaks of single-crystal Si, a graphite peak near 26° is found on the coated Si wafer. However, the relative intensity of the peak is

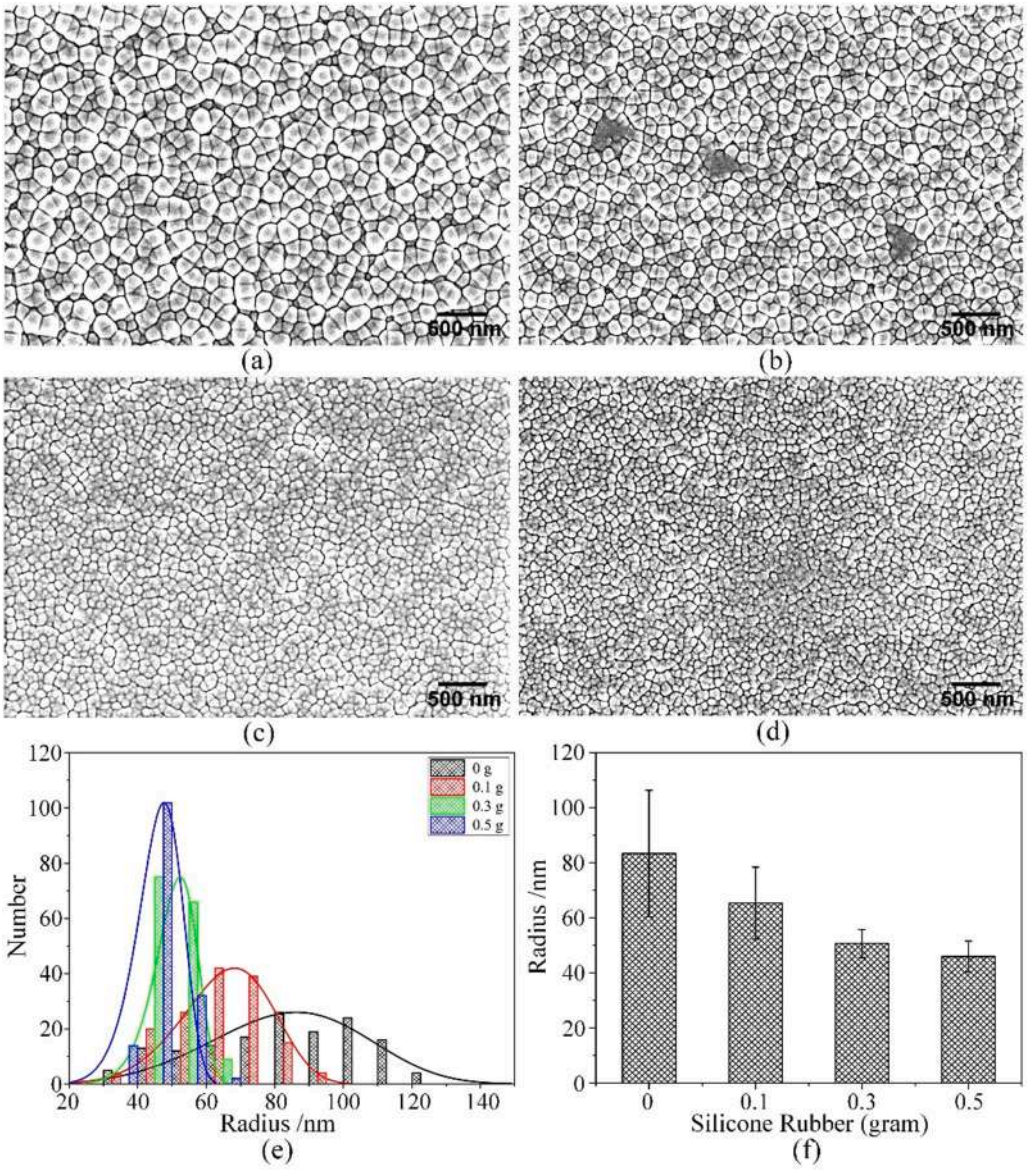

Fig. 5. The grey-scale images of the nano-graphitic carbon coatings with silicone rubber in the APCVD process, (a) 0 g, (b) 0.1 g, (c) 0.3 g, and (d) 0.5 g, (e) statistical analysis of the size distribution of the island-like domains, and (f) average diameter and statistical variance.

weak, which suggests the thickness of the nano-graphitic carbon coating is much smaller than the penetration depth (~1 μm) of the XRD. In addition, it is also noted that with more silicon rubber, the intensity of Si peak on the XRD spectra becomes weaker. It might be due to the better coverage of small spherical carbon clusters on the Si wafer grown with more silicone rubber.

For further investigation on the chemical bonding, the nano-graphitic carbon coatings grown without and with 0.5 g silicone rubber are analyzed using XPS. Fig. 9(a) and (b) show the full-scale XPS spectra of the nano-graphitic carbon coatings. The chemical bonds of the C and O elements can be obtained by XPS spectroscopy. Among them, the high-resolution C 1s peak can be further identified and split into several peaks at approximately 284.0 eV, 285.0 eV, and 288.5 eV, which should correspond to the C═C, C—C, and C═O groups [24,38]. From the intensity of the bonding energy, the high concentration of the C═C bond indicates that in both conditions, the C═C bond takes up a large portion of the nano-graphitic carbon coatings. In addition, the slightly higher ratio of C—C in the case with 0.5 g silicone rubber should be attributed to the effect of atomic impurities. In this work, the nano-graphitic carbon coating mainly consists of C═C bonds, which should belong to graphite-like carbon.

The surface morphologies of the coated and uncoated Si wafers are further characterized by a white-light profilometer. The surface morphology and roughness of the coated and uncoated Si wafers are measured with a magnification ×50, as shown in Fig. 10. From the results, the surface roughness of the nano-graphitic carbon coating in Fig. 10(a) to (d) is S_a 1.8 nm, 1.7 nm, 1.6 nm, and 1.5 nm, respectively. Compared with the uncoated Si wafer surface roughness S_a 1.2 nm, no remarkable differences in the surface roughness are obtained between the coated and uncoated Si wafers. Among these coatings, the surface roughness is slightly enhanced with the introduction of silicone rubber, which could also be confirmed by the AFM micrographs in Fig. 6. Thus, even though the nano-graphitic carbon coating has illustrated great potential as an alternative coating material for glass molding, the surface morphologies should be optimized by carefully modulating the parameters of the APCVD process.

3.2. The effect of growth duration

To optimize the surface nano-morphologies and understand the

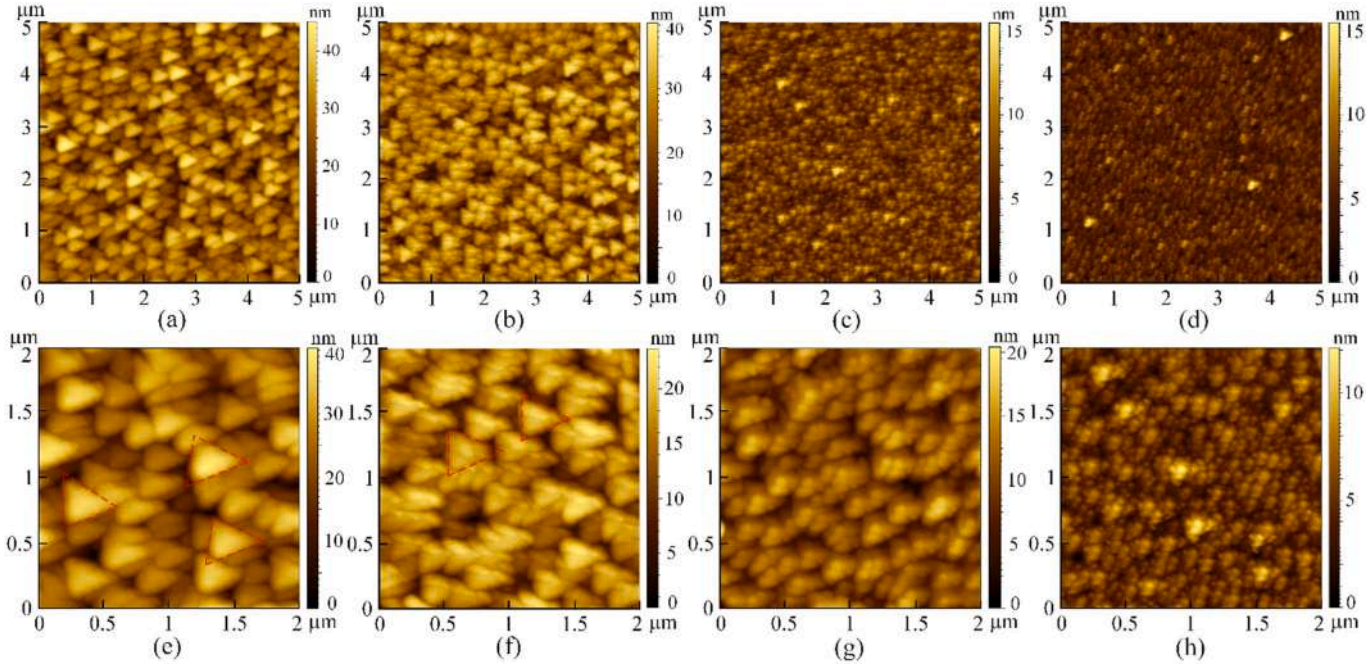

Fig. 6. Characterization of the nano-graphitic carbon coating by AFM with silicone rubber in the APCVD process, (a) and (e) 0 g, (b) and (f) 0.1 g, (c) and (g) 0.3 g, and (d) and (h) 0.5 g. The scan size is 5 μm × 5 μm for (a), (b), (c), and (d) and 2 μm × 2 μm for (e), (f), (g), and (h).

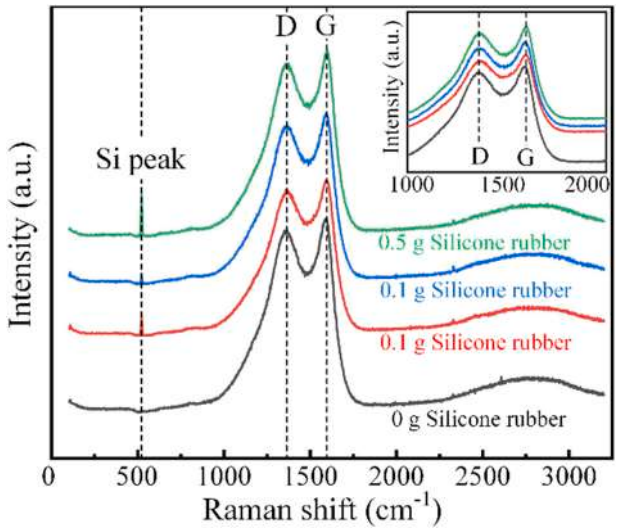

Fig. 7. The Raman spectra obtained from the nano-graphitic carbon coatings grown with and without silicone rubber in the APCVD process.

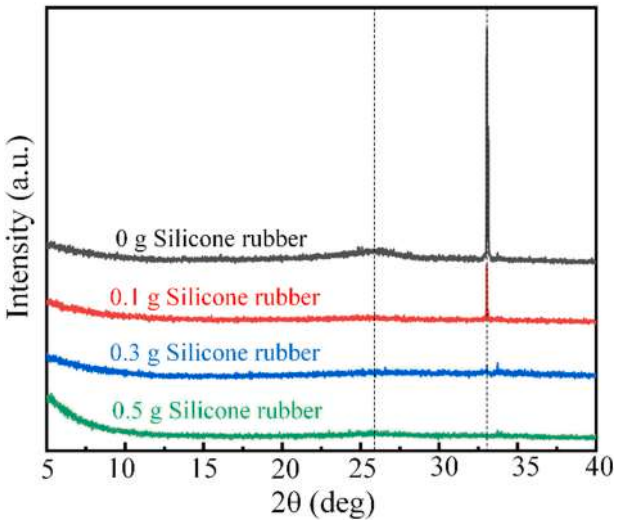

Fig. 8. The XRD spectra obtained from the nano-graphitic carbon coatings grown with and without silicone rubber in the APCVD process.

geometrical evolution of the nano-graphitic carbon coating, a series of experiments with various growth durations are performed on Si wafers. The growth durations are set as 5 mins, 10 mins, 15 mins, and 20 mins. The silicone rubber (0.5 g) and other conditions are the same. Fig. 11 illustrates the SEM micrographs of the nano-graphitic carbon-coated Si wafers with different growth durations. From the above characterization, the introduction of silicone rubber can change the surface morphologies of the nano-graphitic carbon coating. With a large amount of silicone rubber, the particle carbon clusters are promoted rather than the triangle-shaped carbon layers. Once the carbon source is introduced into the tube furnace at the coating temperature, a considerable number of active sites for the carbon clusters appear on the Si wafer in a short time with comparable gaps, as shown in Fig. 11(a). With more amount of carbon sources introduced into the process, as shown in Fig. 11(b) and (c), the gaps between the active nucleation sites are gradually filled up, and these active sites become large enough to coalesce and achieve complete surface coverage, which smoothens the coating surfaces. With further extended growth duration, as shown in Fig. 11(d), these coalesced domains become more significant and protrude from the coating surface, deteriorating the surface's smoothness and flatness.

For further analysis of the morphologies of the nano-graphitic carbon coating, the AFM micrographs of the nano-graphitic carbon coating should be provided. Fig. 12 shows the nano-morphologies of the nano-graphitic carbon coatings with different growth durations. Unlike the nano-morphologies of nano-graphitic carbon coating without silicone rubber, the nano-graphitic carbon coatings grown with 0.5 g silicone rubber are covered with varying particle clusters according to various growth durations. In addition, similar features of the particle clusters shown in Fig. 11(a) and (b), the significant gaps between active sites are

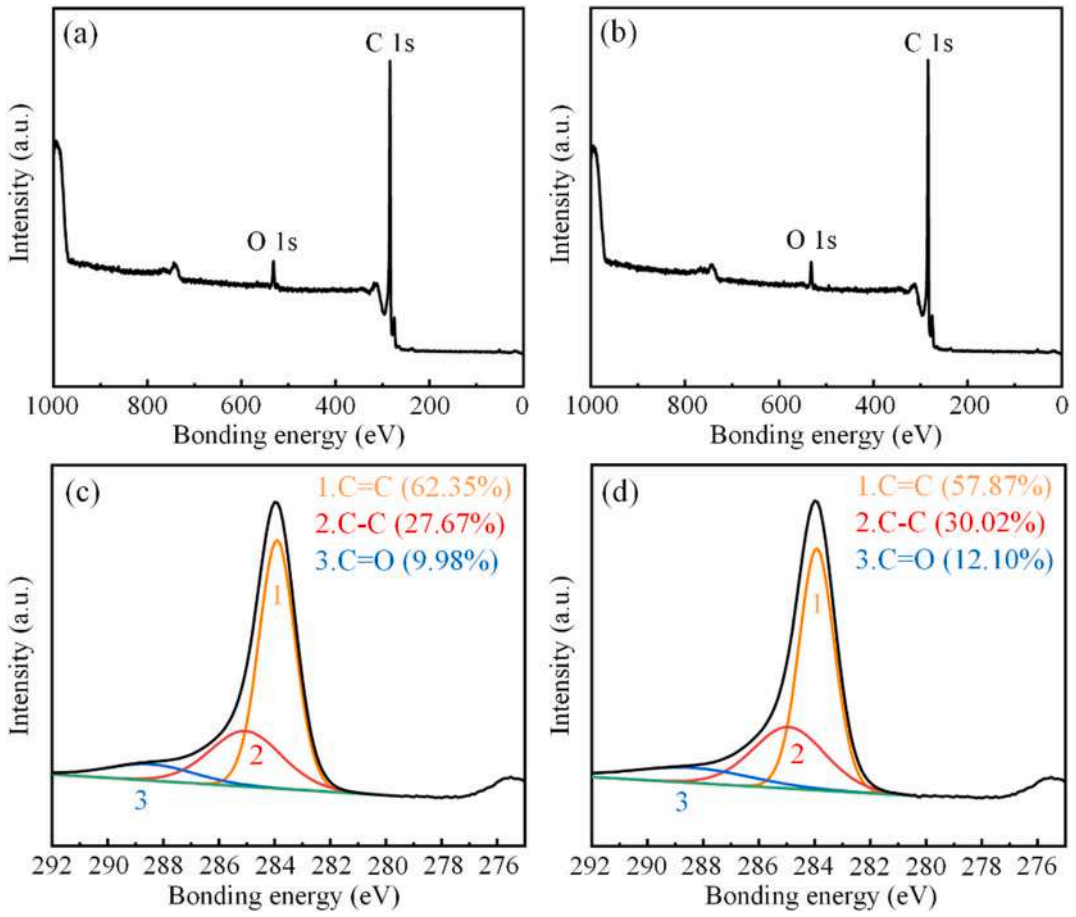

Fig. 9. (a)–(b) XPS full-scale scans of the nano-graphitic carbon coating grown without and with 0.5 g silicone rubber, (c)-(d) high-resolution C 1s spectra analysis of the nano-graphitic carbon coating grown without and with 0.5 g silicone rubber.

further confirmed by the AFM images with the growth durations of 5 mins and 10 mins, shown in Fig. 12(a) and (b). However, when the coating duration is extended above 15 mins, most active sites join, and some coalesce into large carbon clusters, which protrude from the coating surface. Therefore, the morphology evolution of the nano-graphitic carbon coating on the silicon wafer is based on the nucleation of active sites, individual growth, coalescence, and combination, which is entirely different from that in the graphene coating process [38,39].

3.3. Cross-section characterization

To obtain more insight into the structures of the nano-graphitic carbon coating with thickness greater than the penetration depth of Raman spectra, a comparison of nano-graphitic carbon coatings grown with and without silicone rubber is conducted by cross-section observation. The cross-section specimens are prepared by FIB from the nano-graphitic carbon-coated Si wafers grown without and with 0.5 g silicone rubber, which share the same growth duration of 20 mins. The cross-sectional views of the nano-graphitic carbon coating are shown in Fig. 13. From the structures shown in Fig. 13(a) and (c), nanometric thickness carbon coatings have been successfully deposited on the Si wafers and covered a relatively large area in both conditions. From the enlarged views shown in Fig. 13(b) and (d), the thickness and surface morphology of the nano-graphitic carbon coatings grown with and without silicon rubber illustrate remarkable differences. On one hand, there is a noteworthy difference in the thickness of nano-graphitic carbon coatings. Compared with the thickness of nano-graphitic carbon coating grown with silicone rubber (213.5 nm), the thickness of nano-graphitic carbon coating is much larger in the case grown without silicone rubber (329.7 ± 19.5 nm). On the other hand, the nano-graphitic carbon coating grown without silicone rubber forms distinct periodic structures on the top surface. In contrast, the surface of its counterpart with silicone rubber is relatively smooth. More importantly, a visible nanometric transition layer presents between the nano-graphitic carbon coating and the Si substrate, which shares a similar thickness (about 20 nm) in both conditions. Therefore, based on the results, the carbon coating on the Si wafer consists of a nanometric thickness transition layer (about 20 nm) on the bottom and a nano-graphitic carbon coating on the top (>150 nm).

In order to evaluate the transition layer between the nano-graphitic carbon coating and the Si substrate, EDX spectroscopy is utilized to analyze the element layout and the corresponding contents. Among them, silicon, oxygen, and carbon are qualitatively characterized in both the nano-graphitic carbon coating and the transition layer, as shown in Fig. 14. From the results, it is noteworthy that the nano-graphitic carbon layer mainly consists of carbon, and the transition layer consists of silicon, carbon, and oxygen in both conditions, which should be attributed to the residual oxygen and the SiOC source [40]. Compared with the element contents in the transition layers, the oxygen is correlated favorably with the achievable silicone rubber. Since the SiOC is the most crucial backbone of siloxane polymers, it is believed that the SiOC in the transition layer is the deposition of pyrolyzed silicone rubber, which should decompose between 400 °C and 600 °C before the introduction of the carbon source at 1000 °C. Thus, a thin layer consisting of SiOC is initially formed on the Si wafer before the nano-graphitic carbon coating deposition. Apparently, the transition layer acts as a crucial medium in strengthening the covalent bonding and compromising the internal

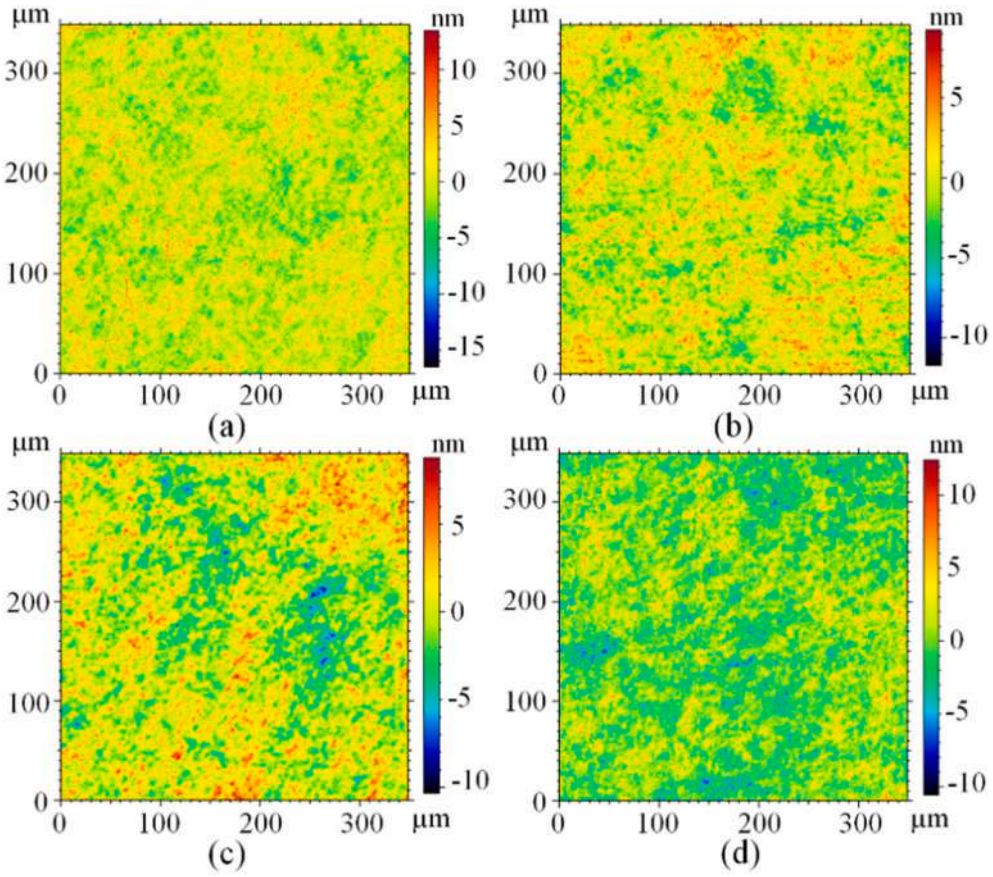

Fig. 10. Surface morphology and roughness of the nano-graphitic carbon coating grown with silicone rubber in the APCVD process, (a) 0 g, (b) 0.1 g, (c) 0.3 g, and (d) 0.5 g.

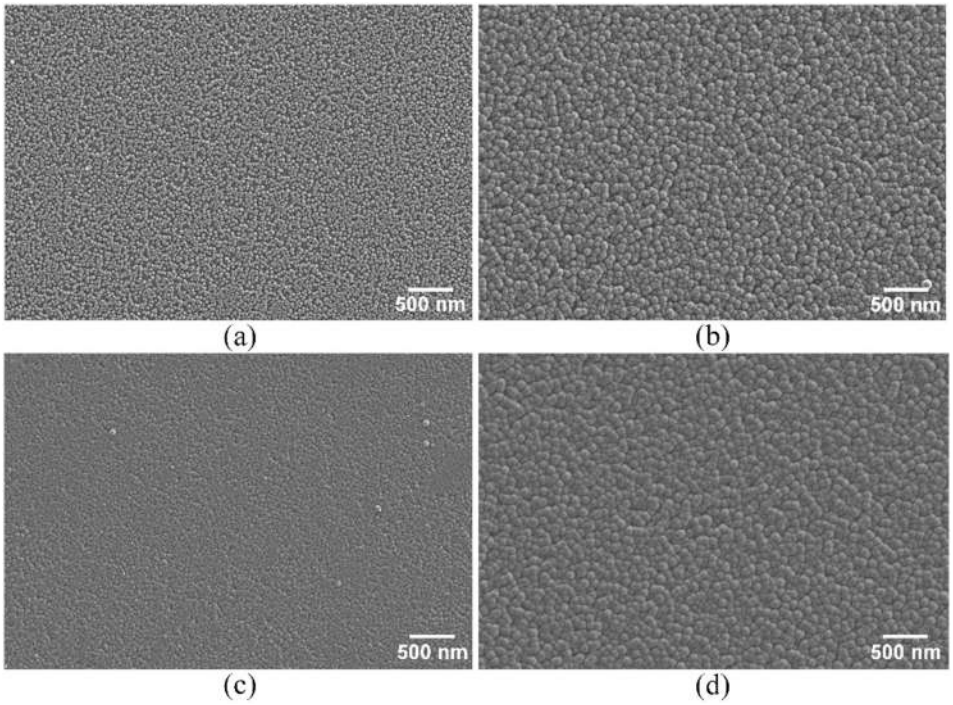

Fig. 11. SEM pictures of the nano-graphitic carbon coating with different growth durations, (a) 5 mins, (b) 10 mins, (c) 15 mins, and (d) 20 mins.

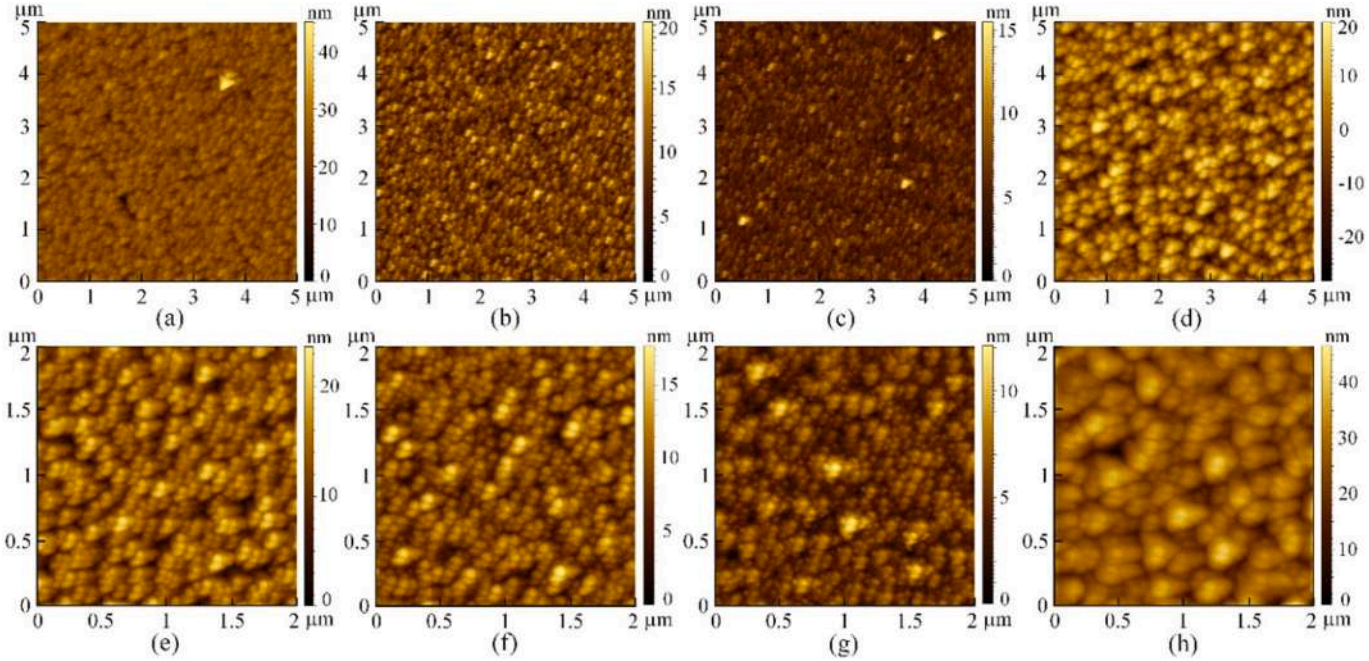

Fig. 12. Characterization of the nano-graphitic carbon coating by AFM with different growth durations (a) and (e) 5 mins, (b) and (f) 10 mins, (c) and (g) 15 mins, and (d) and (h) 20 mins. The scan size is 5 μm × 5 μm for (a), (b), (c), and (d) and 2 μm × 2 μm for (e), (f), (g), and (h).

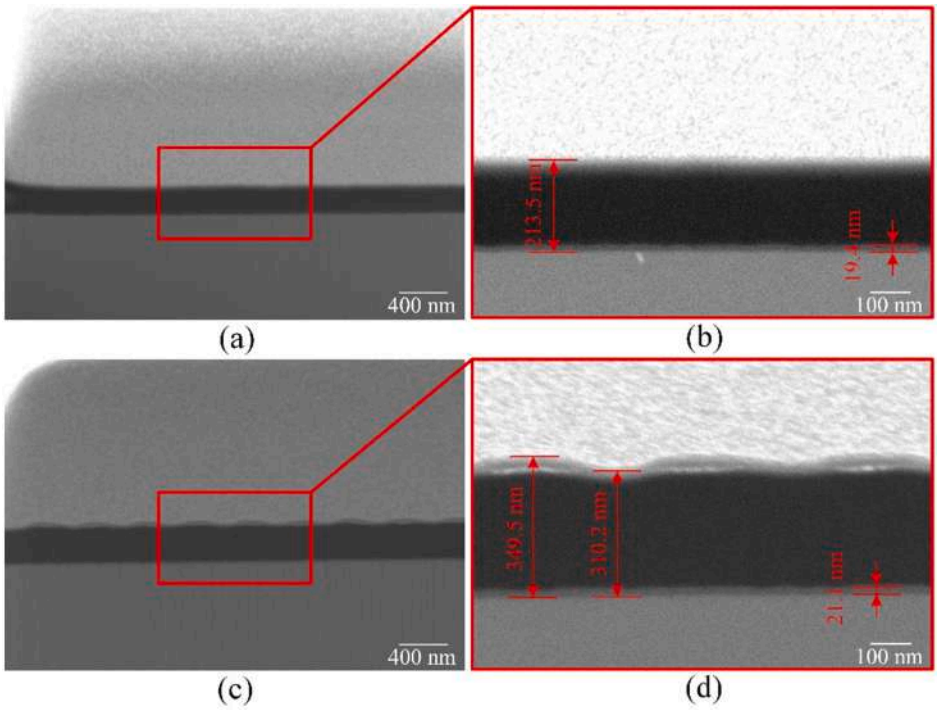

Fig. 13. SEM cross-sectional and enlarged views of the nano-graphitic carbon coatings and interfacial transition layers in the carbon coating grown (a) and (b) with 0.5 g silicone rubber, and (c) and (d) without silicone rubber.

stresses in the coating layer introduced by the thermal expansion/shrinkage and lattice structure mismatch between the nano-graphitic carbon coating and Si substrate [41].

Further analysis of the element mapping along the coating depth is conducted and shown in Fig. 15. From the results, the oxygen content along the interface between the nano-graphitic carbon coating and the Si substrate illustrates significant variation (marked with A). More oxygen element is concentrated in the transition layer when the carbon coating is grown with silicone rubber. It indicates that more SiOC covalent bonds are formed and deposited on the interface due to the silicone rubber. In addition, compared with the case without silicone rubber, the silicon content in the carbon coating is slightly higher in the case with silicone rubber (marked with B). Due to the introduction of the SiOC bonds in the transition layer, there is no need to build transition layers with other ceramic/oxidation materials to enhance the interfacial adhesion [42].

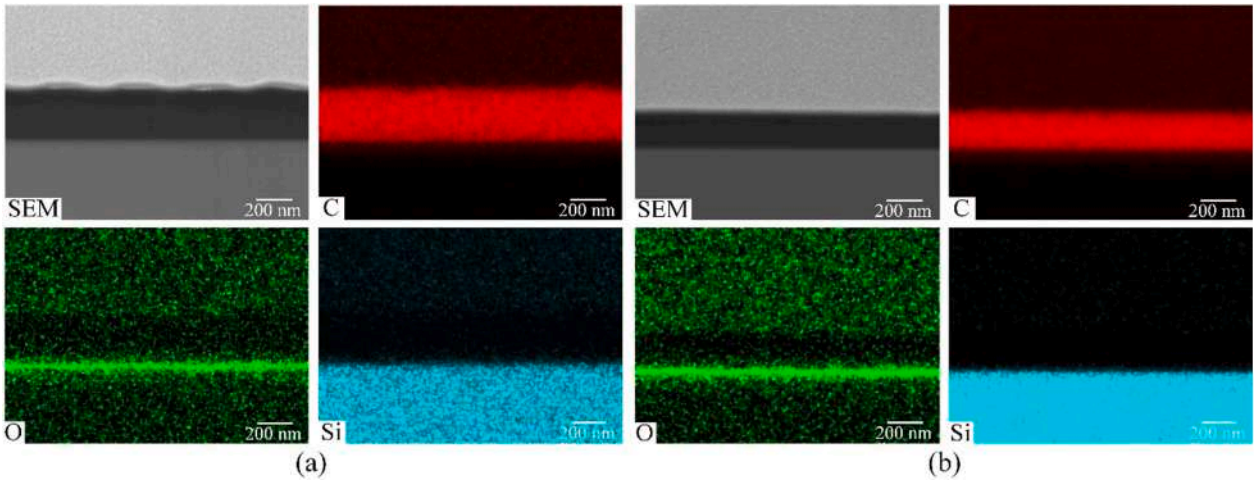

Fig. 14. EDX analysis of the nano-graphitic carbon coating and the transition layer in the carbon coating grown (a) without silicone rubber, and (b) with 0.5 g silicone rubber.

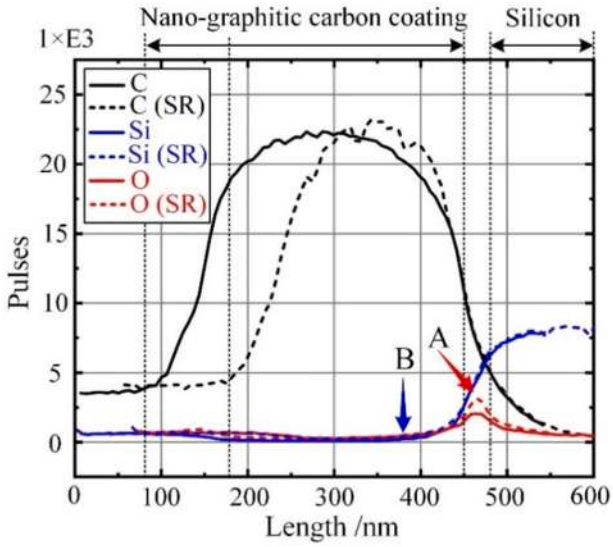

Fig. 15. Element distribution along the nano-graphitic carbon coating depth, including oxygen, silicon, and carbon. The SR in the chart is short of silicone rubber.

3.4. Preliminary molding tests on coated wafer

The nano-graphitic carbon coating is expected to be worked as a non-stick layer to eliminate the direct adhesion between the Si mold insert and glass at elevated temperatures. A few preliminary molding experiments are performed to evaluate the coating strength and the anti-adhesion performance. As shown in Fig. 16(a), a cylinder-shaped K-PG375 glass preform and two Si mold inserts are located in a sandwich style. The variations of molding parameters versus time are illustrated in Fig. 16(b). The glass preform and the molding assemblies are heated by infrared heaters to 370 °C in a protective gas shield and subsequently pressed with a compression force of 500 N for 5 mins. After cooling down, the molded glass is released from the Si mold insert. Fig. 16(c) and (d) show the photographs of the molded glass and the Si mold inserts with and without nano-graphitic carbon coating, respectively. From the results, the coated Si mold insert has successfully changed the glass preform into a disk with a height of 2.0 mm and a diameter of 13.5 mm without visible contamination or failure. In contrast, both the molded glass and the uncoated Si mold insert are broken due to adhesion-induced internal stress. This glass molding experiment demonstrates the feasibility of nano-graphitic carbon coating in eliminating the interfacial adhesion between Si mold insert and glass at elevated temperatures.

Furthermore, the durability and surface micro/nano-morphology evolution of the nano-graphitic carbon coating in repetitive thermal and mechanical treatments should be investigated. To do this, repetitive molding experiments are performed on the nano-graphitic carbon-coated Si mold inserts. Fig. 17 shows the surface morphologies of the nano-graphitic carbon coating after 35 times repetitive glass molding. From the micro-morphologies shown in Fig. 17(a) and (c), the average surface roughness of the Si mold insert and molded glass is about S_a 1.4 nm and 1.5 nm, which is very close to the initial surface roughness of the coated Si mold insert. In addition, there are no emerging signs of adhesion, separation, or failure on the nano-graphitic carbon coating. Furthermore, the homogeneous micro-morphologies of the nano-graphitic carbon coating after repetitive molding experiments illustrate similar surface features, as shown in Fig. 12(g).

The nano-morphologies of the Si mold insert and molded glass after multiple molding experiments are also provided, since it is crucial to reveal the interface mechanism in glass molding. From the measured results in Fig. 17(b) and (d), the reverse nano-structures cover most areas of the molded glass. Besides the surface nano-structures, the microscale bubble (marked with A) with some inside scratches (marked with B) due to the polishing process before molding occasionally appears on the molded surface. This defect should be attributed to the concentration of trapped air in the glass molding.

In addition, a series of durability tests are conducted with high transition temperature oxide glass P-SK57 to evaluate the nano-graphitic carbon coating. In the experiments, the pressing phase is deliberately elongated to 15 mins under 550 °C and 2.0 kN load, which is long enough for the potential interfacial diffusion between the glass and the nano-graphitic carbon coating at elevated temperatures. The molding experiments are repeated 5 times on one set of coated molds. After molding tests, the molded glass and the silicon molds are directly observed without further processing. The photography of the molded glass and Si mold is illustrated in Fig. 18(a). There is no visible contamination or failure on the nano-graphitic carbon coating as well as the P-SK57 glass, which is further confirmed by the SEM observation of the nano-graphitic carbon coating in Fig. 18(b). Furthermore, an arbitrary region of the nano-graphitic carbon coating is captured by a white-light interferometer with a magnification ×50 and shown in Fig. 18(c). From the measured results, the surface shows similar characteristics of morphology and roughness (S_a 1.7 nm) as before molding. Finally, in

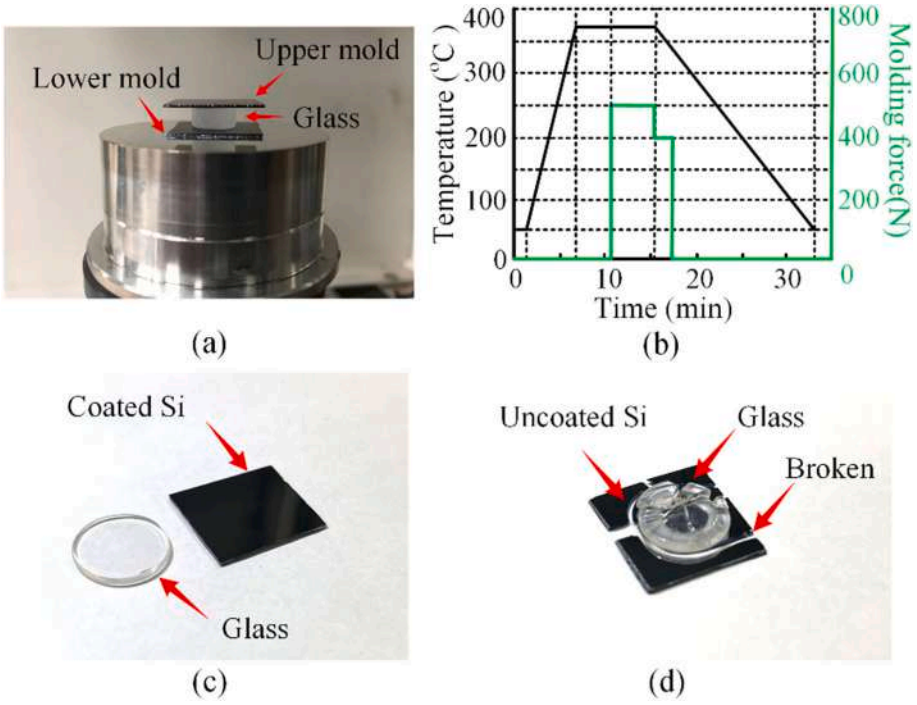

Fig. 16. (a) Cross-section view of the glass molding experiment setup, (b) temperature and load history of glass molding, glass molding using (c) coated Si wafer, and uncoated Si wafer.

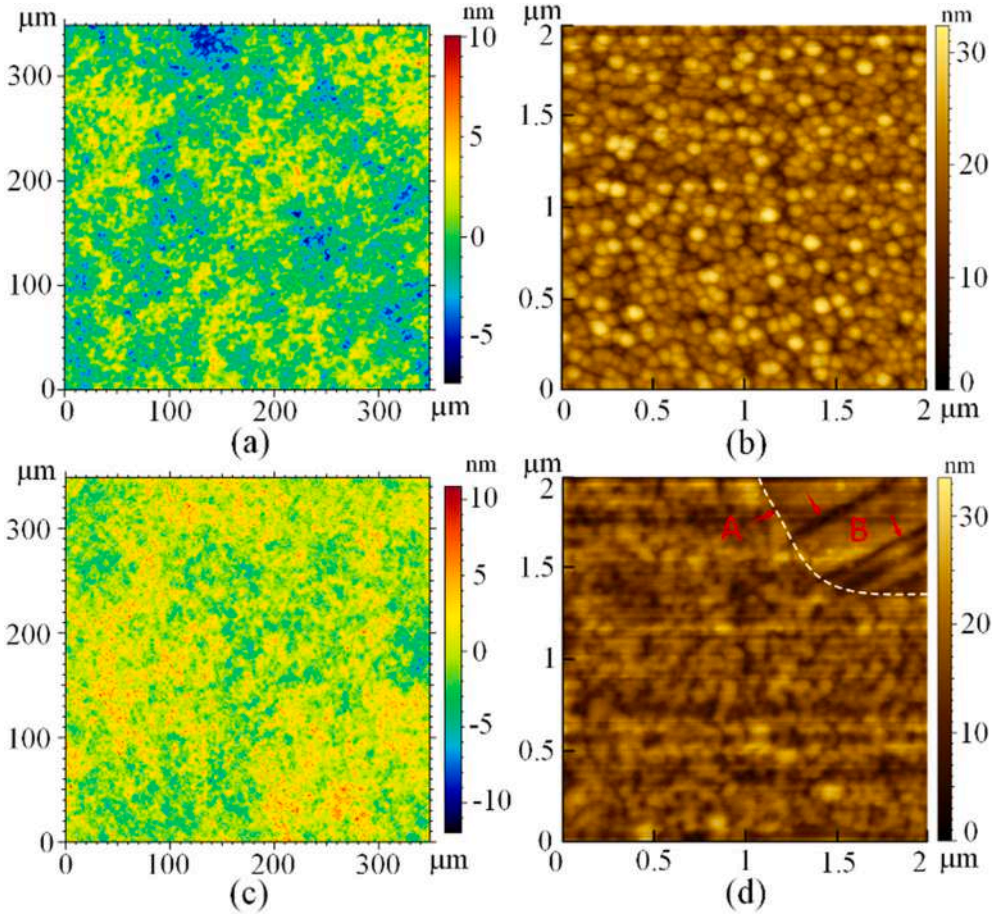

Fig. 17. Surface micro/nano-morphologies of (a) and (b) the coated Si wafer, (c) and (d) molded glass surface after multiple glass molding tests.

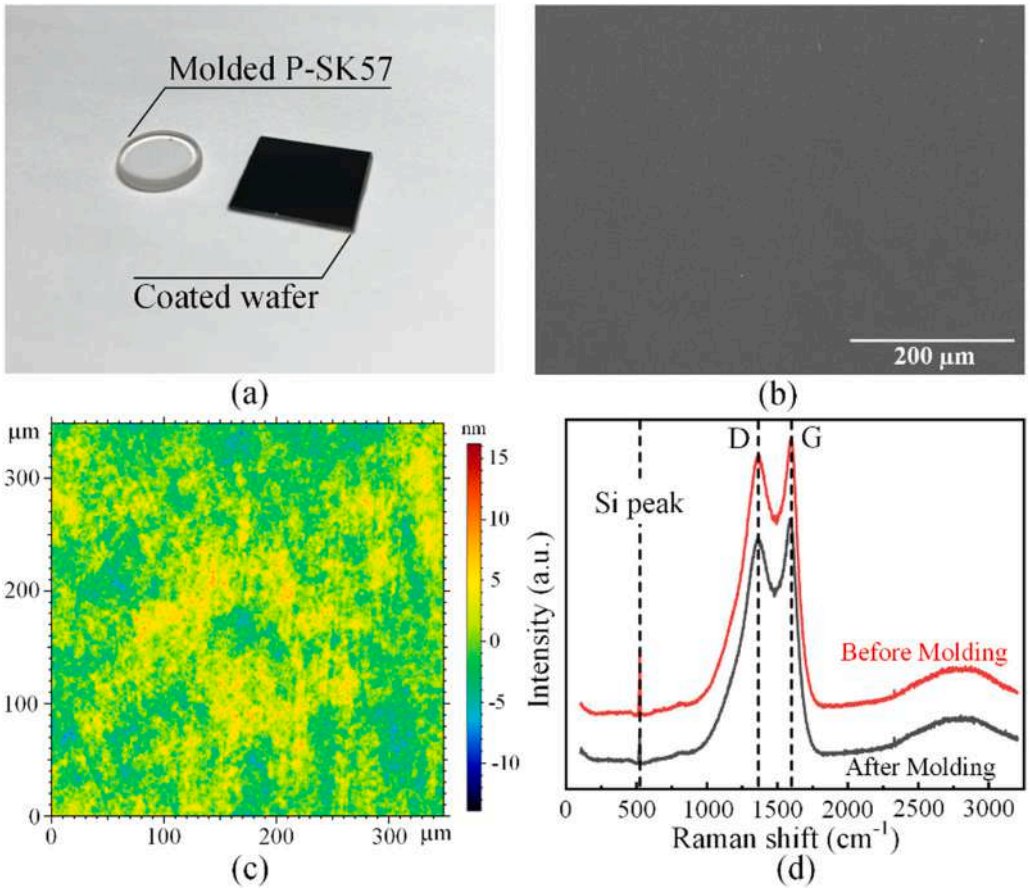

Fig. 18. Surface characterization of the nano-graphitic carbon coating after durability tests, (a) photography of the molded glass and Si mold, (b) SEM image of the nano-graphitic carbon coating, (c) 3D morphology of the nano-graphitic carbon coating, and (d) comparison of Raman spectra for the nano-graphitic carbon coating before and after molding tests.

order to confirm that no graphitization or degradation occurred, the Raman spectra of the nano-graphitic carbon coating are compared before and after molding tests, as shown in Fig. 18(d). The D and G peaks share almost the same features with no translation and position distortions, which indicates that the lattice structure of the nano-graphitic carbon coating keeps the same.

The element diffusion and concentration at elevated temperature is a potential phenomenon that might occur in glass molding, which is typical for metallic coating materials [43]. Fig. 19 shows the element distribution of the nano-graphitic carbon coating on the Si wafer before and after durability tests. The obtained results reveal no sign of element concentration or diffusion on the carbon-coated surface during the molding process. In addition, compared to the element contents, including the silicon, oxygen, and carbon element listed in Table 1, the element ratio is almost the same (difference < 1.5 %), which indicates no noticeable content variation in the cyclic molding tests. The experiments suggest that the nano-graphitic carbon coating has adequate strength and durability in mechanical and thermal cycles, which could be adopted for most molding experiments (molding temperature $<$ 550 °C).

Based on the above experiments, the interfacial mechanism between the coated Si mold insert and glass preform in precision glass molding can be summarized in Fig. 20. Before molding, the micro/nano-structures on the mold insert and glass preform result in a large number of gaps between the interfaces, which are filled with air. As the molding assemblies are heated up, and the glass substrate changes into the viscoelastic state, the external pressure applied to the mold insert drives the softened glass to fill the gaps. In principle, the micro/nano-structured interfaces in precision glass molding result in three kinds of typical phenomena in surface generation, which can be summarized as follows,

(I) Well-contact and perfect replication. Suppose the trapped air is entirely exhausted from the micro/nanoscale spaces. In that case, the viscoelastic glass can be gradually squeezed to closely match the surface profile of the mold insert without any defects. This should be the optimal condition in precision glass molding.
(II) Partial filling due to nanoscale bubble. Unlike the conditions stated above, this defect is due to the initial trapped air, which fails to exhaust from the micro/nanoscale gaps prior to precision glass molding. As the trapped air inside the enclosed gaps is compressed to similar or even larger than the external pressure, the viscoelastic glass can no longer fill out the gaps.
(III) Micro-bubble on the contact surface. This kind of surface defect is common in precision glass molding, when the experiment is conducted in air conditions. It should be attributed to the trapped gas gathered together and left between the interfaces. These micro-bubbles, usually several to tens of micrometers, impede the undergoing filling of viscoelastic glass on the interface, and the initial defects on the glass surface remain on the bottom of these micro-bubbles.

3.5. *Precision glass optics molding*

Further evaluation of the effectiveness of the nano-graphitic carbon coating on micro-patterned Si mold inserts is conducted. The micro-pillar matrix, a binary micro-pattern, is fabricated with UV lithography followed by the RIE process. After the Si mold insert is coated with

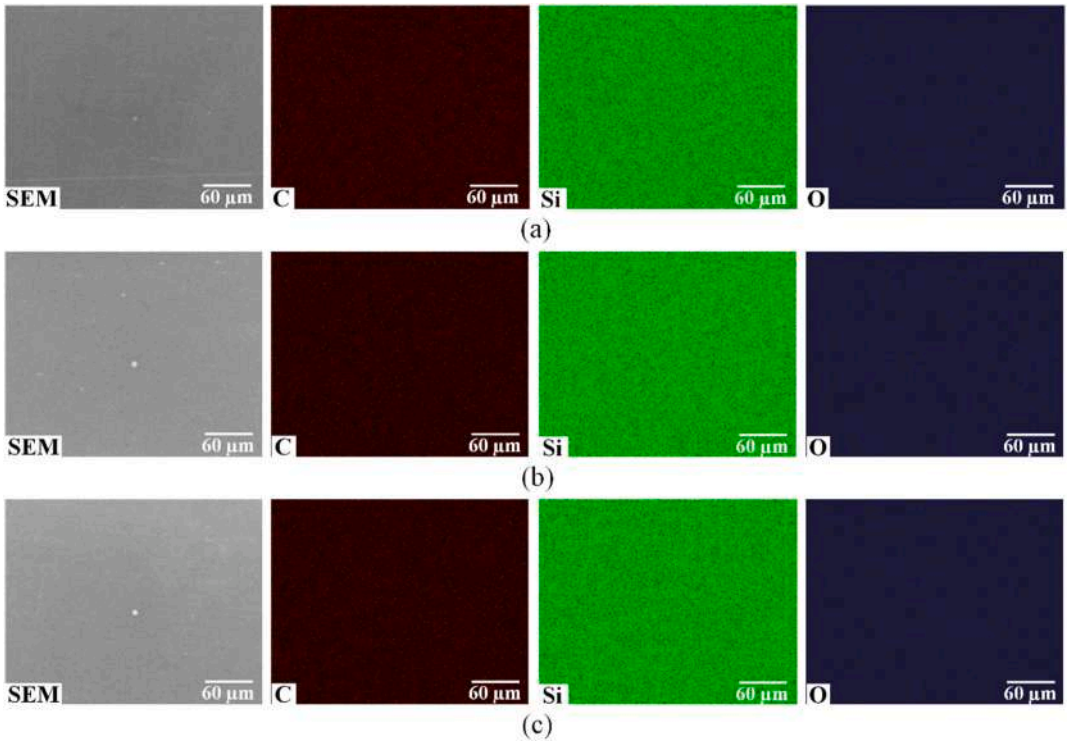

Fig. 19. EDS elemental mapping images of the Si wafer with nano-graphitic carbon coating (a) before molding, (b) after 35 molding tests at 370 °C, and (c) after 5 molding tests at 550 °C.

Table 1
Element contents in the carbon coatings (atomic percentage).

	Carbon	Oxygen	Silicon
Before molding test	50.06	1.67	48.27
After 35 molding tests with 370 °C	48.53	1.85	49.62
After 5 molding tests with 550 °C	50.91	1.94	47.14

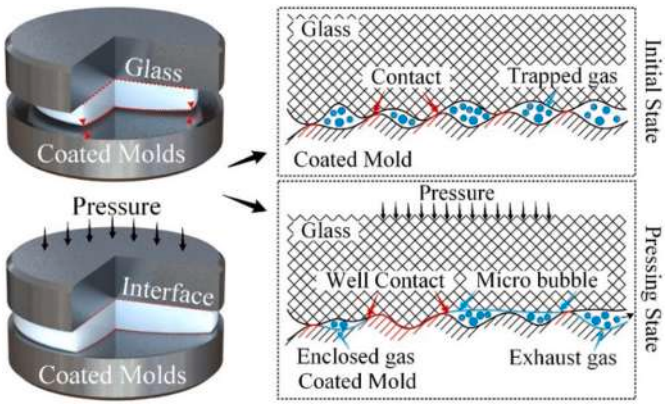

Fig. 20. Schematic diagrams of the micro/nano-structures formation during the glass molding using nano-graphitic carbon-coated Si mold insert.

a nano-graphitic carbon coating by the APCVD, the micrograph and morphology by SEM and optical profilometer are shown in Fig. 21(a) and (b). The results show that the micro-pillar matrix has an interval of 10 μm and a height of 450 nm. After the micro-pattern on the Si mold insert has been transferred to the glass substrate by precision glass molding, the 3D morphology of the micro-pattern is measured and shown in Fig. 21(c). The corresponding cross-sectional profiles of the Si mold insert and the molded glass are extracted and shown in Fig. 21(d). The average depth of the micro-well matrix is about 445 nm, and the distance between the successive micro features is about 9.96 μm. The observed values show good agreement with the Si mold insert measured above. In addition, the surface profiles, as well as the surface integrity, match well with each other, showing high consistency and high accuracy of the obtained microstructures.

The uniformity and smooth finish surface of the nano-graphitic carbon coating indicate that it is possible to be used as an anti-adhesion coating in high-precision glass optics molding. As a proof-of-concept, a hexagonal micro-lens array is further employed as a mold insert in high-precision glass optics molding. The micrograph and the 3D morphology of the hexagonal micro-lens array on the coated Si mold insert are presented in Fig. 22(a) and (b). From the obtained results, it is clear that the concave lenslets are uniformly located inside a circle of the Si mold insert. As illustrated in Fig. 22(c), the 3D morphology of the micro-lens array on the molded glass is achieved by the optical profilometer. For further evaluating the replication fidelity, the cross-sectional profile of the micro-lens array is extracted to characterize the fidelity, as shown in Fig. 22(d). Compared with the Si mold insert, homogeneous features of the micro-lens array on the molded glass are achieved by precision glass molding without significant distortion or variation. The cross-sectional profiles of the Si mold insert and the molded glass agree well with each other. The obtained form errors are less than ±100 nm, which confirms the feasibility of nano-graphitic carbon coating in high-precision glass optics molding.

After molding, the micro-patterned Si mold inserts with nano-graphitic carbon coating show no sign of wearing or changes in surface roughness. The molding experiments with flat and micro-patterned coated Si mold inserts have confirmed that the nano-graphitic carbon coating has enough durability and high surface integrity for high-precision glass optics molding.

3.6. Optical performance

The optical focusing performance of the molded glass micro-lens

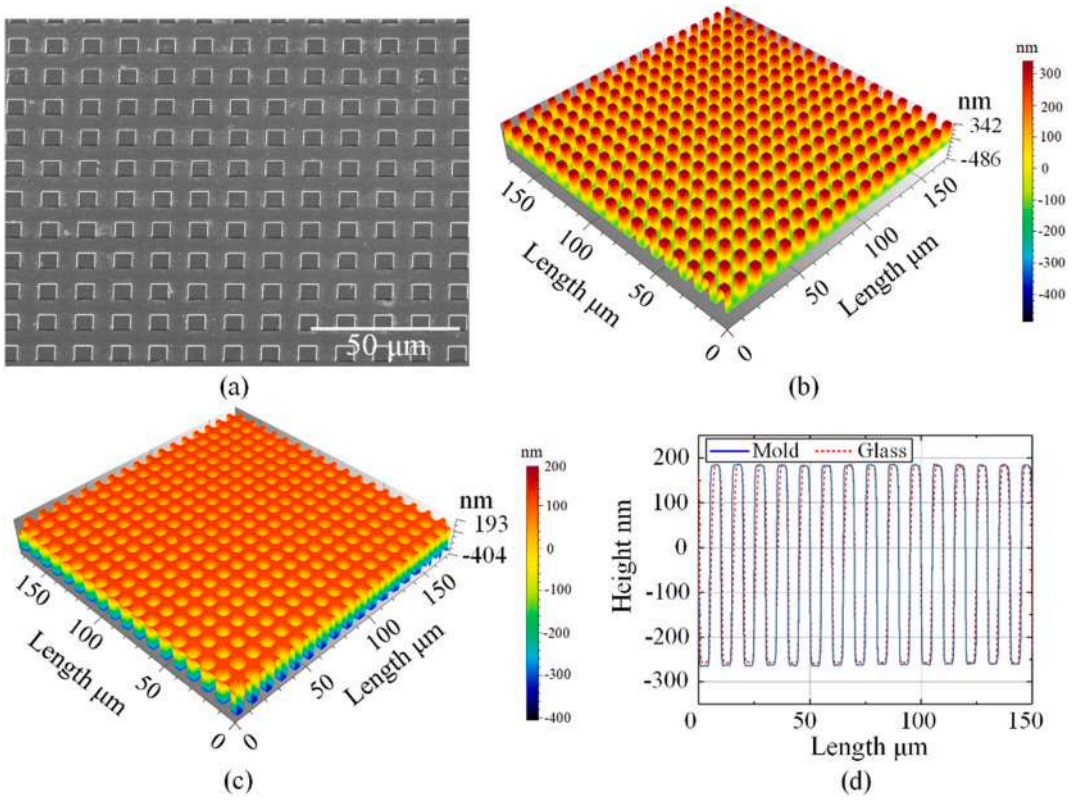

Fig. 21. (a) SEM pictures of the micro-pillar matrix on the coated Si mold insert, (b) 3D morphology of the micro-pattern on coated Si mold insert, (c) 3D morphology of the micro-pattern on molded glass, and (d) comparison of cross-section profiles between the coated Si mold insert and the molded glass.

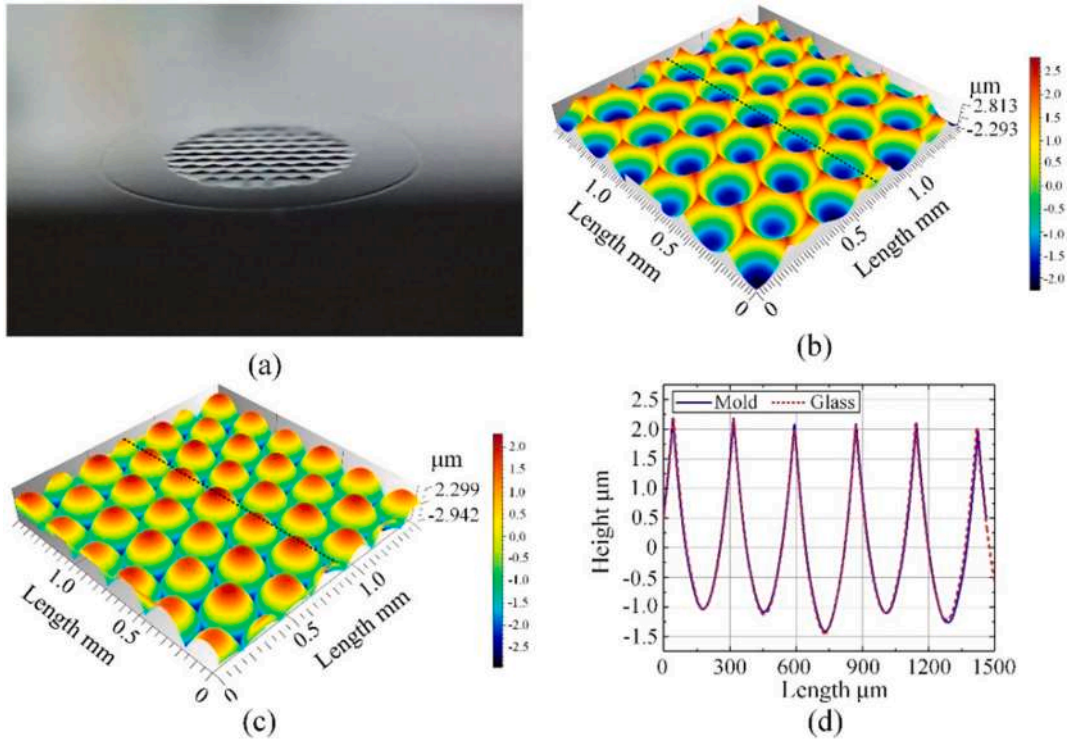

Fig. 22. (a) Photograph of the concave micro-lens array on the coated Si mold insert, (b) 3D morphology of the micro-pattern on the coated Si mold insert, (c) 3D morphology of the micro-pattern on molded glass, and (d) comparison of cross-section profiles between the coated Si mold insert and the molded glass.

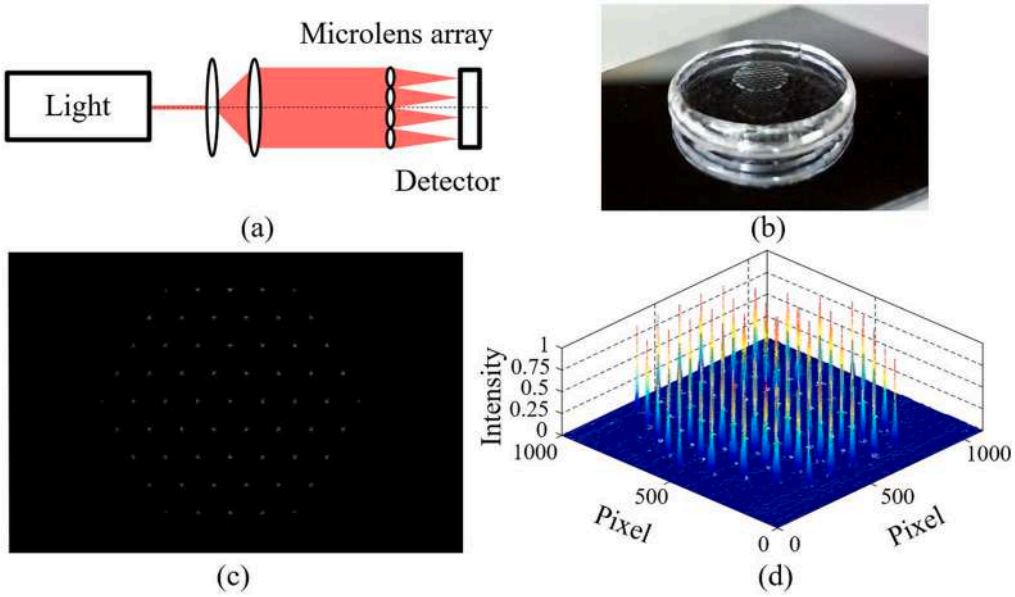

Fig. 23. (a) Optical apparatus for testing the optical performance of the molded micro-lens array, (b) photography of the molded micro-lens array, (c) raw image of the spot pattern on the CCD detector, and (d) the light intensity of the spot pattern.

array is evaluated using an optical apparatus, as illustrated in Fig. 23(a). The light source employed in the optical test is a white light bulb, which is further collimated by a pair of double-convex lenses. A beam of parallel light is projected to the molded micro-lens array, as shown in Fig. 23(b). By adjusting the distance between the micro-lens array and the detector, the focal spot pattern is formed on the sensor. The captured raw image is illustrated in Fig. 23(c). Furthermore, the intensity of the micro-lenses is extracted from the spot pattern and shown in Fig. 23(d). The normalized light intensity of the spot pattern was between 0.973 and 0.998, indicating the homogenous optical property of the molded micro-lens array.

4. Conclusion

In summary, we demonstrate a fast and cost-effective method for producing nanometric nano-graphitic carbon coating directly on Si wafer using APCVD. The surface micro/nano-morphologies can be tuned by modulating the element contents or changing the growth durations. The SEM and AFM micrographs confirm that the presence of modifying elements, the SiOC source, in the APCVD can affect the growth mode of nano-graphitic carbon, which leads to different micro/nano-morphologies of the coatings. In addition, the existence of the transition layer, consisting of silicon, oxygen, and carbon elements, between the nano-graphitic carbon coating and the Si substrate drastically enhances the interfacial adhesion between them and modulates the thermal stresses in the nano-graphitic carbon coating as well. Furthermore, it is worth noting that the nano-graphitic carbon coating is a cost-effective technique compared with the other conventional coating methods, including the cost of coating material and the instrument in the coating process. The proposed method provides a possible approach to producing a solid and thermal stable carbon-based coating on semiconductive substrates without utilizing metal catalysts.

Moreover, the nano-graphitic carbon coating is introduced as an anti-adhesive coating on Si mold inserts to prevent Si-glass adhesion in repetitive molding cycles. This newly developed coating is successfully implemented to replicate two typical micro features on glass substrates with high precision and replication fidelity. Based on the nano-morphologies on the molded glass, the interfacial contact mechanism between the coated Si mold insert and the glass is clearly proposed. By optimizing the molding conditions, high-precision glass micro-optics, such as micro-lens array, can be molded using the nano-graphitic carbon-coated Si mold inserts. In industrial applications, the same strategy can be applied to other non-metallic materials, such as SiC, SiO_2, and Al_2O_3, which are expected to realize their potential as mold materials to improve the machining efficacy and product quality.

CRediT authorship contribution statement

Lin Zhang: Data curation, Investigation, Writing – original draft. **Jiwang Yan:** Conceptualization, Methodology, Supervision, Writing – review & editing.

Declaration of competing interest

The authors declare that they have no known competing financial interests or personal relationships that could have appeared to influence the work reported in this paper.

Data availability

No data was used for the research described in the article.

Acknowledgments

Lin Zhang is an International Research Fellow of the Japan Society for the Promotion of Science (JSPS) (ID No. is P 20368). This study has been financially supported by Grant-in-Aid for JSPS Fellows. Jiwang Yan would like to thank the financial support from Japan Society for the Promotion of Science (JSPS), Grant-in-Aid for Scientific Research (B), project number 21H01230.

References

[1] T. Zhou, Y. He, T. Wang, Z. Zhu, R. Xu, Q. Yu, B. Zhao, W. Zhao, P. Liu, X. Wang, A review of the techniques for the mold manufacturing of micro/nanostructures for precision glass molding, Int. J. Extreme Manuf. 3 (2021), 042002.
[2] L. Li, G. Yang, W.B. Lee, M.C. Ng, K.L. Chan, Carbide-bonded graphene-based joule heating for embossing fine microstructures on optical glass, Appl. Surf. Sci. 500 (2020), 144004.
[3] L. Zhang, A.Y. Yi, Investigation of mid-infrared rapid heating of a carbide-bonded graphene coating and its applications in precision optical molding, Opt. Express 29 (2021) 30761–30771.

[4] L. Zhang, A. Zolfaghari, W. Zhou, Y. Shu, A.Y. Yi, Flexible metallic mold based precision compression molding for replication of micro-optical components onto non-planar surfaces, Precis. Eng. 76 (2022) 149–159.
[5] P. He, L. Li, J. Yu, W. Huang, Y.-C. Yen, L.J. Lee, A.Y. Yi, Graphene-coated si mold for precision glass optics molding, Opt. Lett. 38 (2013) 2625–2628.
[6] Z. Zhu, S. To, S. Zhang, Large-scale fabrication of micro-lens array by novel end-fly-cutting-servo diamond machining, Opt. Express 23 (2015) 20593–20604.
[7] J. Yan, T. Asami, H. Harada, T. Kuriyagawa, Fundamental investigation of subsurface damage in single crystalline silicon caused by diamond machining, Precis. Eng. 33 (2009) 378–386.
[8] A.R. Abdul Manaf, J. Yan, Improvement of form accuracy and surface integrity of si-HDPE hybrid micro-lens arrays in press molding, Precis. Eng. 47 (2017) 469–479.
[9] P. Xie, P. He, Y.-C. Yen, K.J. Kwak, D. Gallego-Perez, L. Chang, W.-C. Liao, A. Yi, L. J. Lee, Rapid hot embossing of polymer microstructures using carbide-bonded graphene coating on silicon stampers, Surf. Coat. Technol. 258 (2014) 174–180.
[10] C.-L. Chao, C.-B. Huo, W.-C. Chou, Y.-R. Lin, K.-J. Ma, H.-H. Chien, Study on the design of precious metal based protective films for glass moulding process, Surf. Coat. Technol. 231 (2013) 567–572.
[11] Y.-I. Chen, S.-M. Chen, Annealing effects on nanostructure and mechanical properties of nanolaminated Ta–Zr coatings, Surf. Coat. Technol. 215 (2013) 209–217.
[12] K.D. Fischbach, K. Georgiadis, F. Wang, O. Dambon, F. Klocke, Y. Chen, A.Y. Yi, Investigation of the effects of process parameters on the glass-to-mold sticking force during precision glass molding, Surf. Coat. Technol. 205 (2010) 312–319.
[13] M. Friedrichs, Z. Peng, T. Grunwald, M. Rohwerder, B. Gault, T. Bergs, PtIr protective coating system for precision glass molding tools: design, evaluation and mechanism of degradation, Surf. Coat. Technol. 385 (2020), 125378.
[14] J. Sakurai, S. Hata, R. Yamuchi, M. Abe, A. Shimokohbe, Searching for Pt–Zr–Ni thin film amorphous alloys for optical glass lenses molding materials, Precis. Eng. 34 (2010) 431–439.
[15] X.-Y. Zhu, J.-J. Wei, L.-X. Chen, J.-L. Liu, L.-F. Hei, C.-M. Li, Y. Zhang, Anti-sticking re-ir coating for glass molding process, Thin Solid Films 584 (2015) 305–309.
[16] Y. Zhang, G. Yan, K. You, F. Fang, Study on α-Al2O3 anti-adhesion coating for molds in precision glass molding, Surf. Coat. Technol. 391 (2020), 125720.
[17] G. Kleer, W. Doell, Ceramic multilayer coatings for glass moulding applications, Surf. Coat. Technol. 94–95 (1997) 647–651.
[18] C.-H. Lin, J.-G. Duh, B.-S. Yau, Processing of chromium tungsten nitride hard coatings for glass molding, Surf. Coat. Technol. 201 (2006) 1316–1322.
[19] D. Zhong, E. Mateeva, I. Dahan, J.J. Moore, G.G.W. Mustoe, T. Ohno, J. Disam, S. Thiel, Wettability of NiAl, ni-Al-N, ti-B-C, and ti-B-C-N films by glass at high temperatures, Surf. Coat. Technol. 133–134 (2000) 8–14.
[20] H. Li, P. He, J. Yu, L.J. Lee, A.Y. Yi, Localized rapid heating process for precision chalcogenide glass molding, Opt. Lasers Eng. 73 (2015) 62–68.
[21] J. Zhou, P. He, J. Yu, L.J. Lee, L. Shen, A.Y. Yi, Investigation on the friction coefficient between graphene-coated silicon and glass using barrel compression test, J. Vac. Sci. Technol. B 33 (2015), 031213.
[22] J. Yan, T. Oowada, T. Zhou, T. Kuriyagawa, Precision machining of microstructures on electroless-plated NiP surface for molding glass components, J. Mater. Process. Technol. 209 (2009) 4802–4808.
[23] A.K. Geim, K.S. Novoselov, The rise of graphene, Nat. Mater. 6 (2007) 183–191.
[24] K. Li, G. Xu, X. Wen, J. Zhou, F. Gong, High-temperature friction behavior of amorphous carbon coating in glass molding process, Friction 9 (2021) 1648–1659.
[25] L. Zhang, W. Zhou, A.Y. Yi, Rapid localized heating of graphene coating on a silicon mold by induction for precision molding of polymer optics, Opt. Lett. 42 (2017) 1369–1372.
[26] J. Vetter, 60years of DLC coatings: historical highlights and technical review of cathodic arc processes to synthesize various DLC types, and their evolution for industrial applications, Surf. Coat. Technol. 257 (2014) 213–240.
[27] W. Huang, X. Ouyang, L.J. Lee, High-performance nanopapers based on benzenesulfonic functionalized graphenes, ACS Nano 6 (2012) 10178–10185.
[28] J. Yan, K. Syoji, T. Kuriyagawa, H. Suzuki, Ductile regime turning at large tool feed, J. Mater. Process. Technol. 121 (2002) 363–372.
[29] M. Mukaida, J. Yan, Fabrication of hexagonal microlens arrays on single-crystal silicon using the tool-servo driven segment turning method, Micromachines 8 (2017) 323.
[30] P. He, F. Wang, L. Li, K. Georgiadis, O. Dambon, F. Klocke, A.Y. Yi, Development of a low cost high precision fabrication process for glass hybrid aspherical diffractive lenses, J. Opt. 13 (2011), 085703.
[31] G. Hong, Q.-H. Wu, J. Ren, S.-T. Lee, Mechanism of non-metal catalytic growth of graphene on silicon, Appl. Phys. Lett. 100 (2012), 231604.
[32] Y. Kim, W. Song, S.Y. Lee, C. Jeon, W. Jung, M. Kim, C.Y. Park, Low-temperature synthesis of graphene on nickel foil by microwave plasma chemical vapor deposition, Appl. Phys. Lett. 98 (2011), 263106.
[33] S. Neuville, Selective carbon material engineering for improved MEMS and NEMS, Micromachines 10 (2019) 539.
[34] K.-B. Kim, C.-M. Lee, J. Choi, Catalyst-free direct growth of triangular Nano-graphene on all substrates, J. Phys. Chem. C 115 (2011) 14488–14493.
[35] G. Irmer, A. Dorner-Reisel, Micro-raman studies on DLC coatings, Adv. Eng. Mater. 7 (2005) 694–705.
[36] A. Hashimoto, K. Suenaga, A. Gloter, K. Urita, S. Iijima, Direct evidence for atomic defects in graphene layers, Nature 430 (2004) 870–873.
[37] S. Neuville, Quantum electronic mechanisms of atomic rearrangements during growth of hard carbon films, Surf. Coat. Technol. 206 (2011) 703–726.
[38] P.D. Garman, H. Yang, Y.-C. Yen, J. Yu, K.J. Kwak, V. Malkoc, V.V. Talesara, L. J. Lee, W. Lu, SiOC-accelerated graphene grown on SiO2/Si with tunable electronic properties, Phys. Status Solidi RRL 13 (2019), 1900017.
[39] P.D. Garman, J.M. Johnson, V. Talesara, H. Yang, X. Du, J. Pan, D. Zhang, J. Yu, E. Cabrera, Y.-C. Yen, J. Castro, W. Lu, J.-C. Zhao, J. Hwang, L.J. Lee, Dual silicon oxycarbide accelerated growth of well-ordered graphitic networks for electronic and thermal applications, Adv. Mater. Technol. 4 (2019), 1800324.
[40] P.D. Garman, Chemical Vapor Deposition of Silicon Oxycarbide Catalyzed Graphene Networks, The Ohio State University, 2018.
[41] P.D. Garman, J.M. Johnson, V. Talesara, H. Yang, D. Zhang, J. Castro, W. Lu, J. Hwang, L.J. Lee, Silicon oxycarbide accelerated chemical vapor deposition of graphitic networks on ceramic substrates for thermal management enhancement, ACS Appl. Nano Mater. 2 (2019) 452–458.
[42] V. Talesara, P.D. Garman, J.L. Lee, W. Lu, Thermal management of high-power switching transistors using thick CVD-grown graphene nanomaterial, IEEE Trans. Power Electron. 35 (2020) 578–590.
[43] J. Masuda, J. Yan, T. Zhou, T. Kuriyagawa, Y. Fukase, Thermally induced atomic diffusion at the interface between release agent coating and mould substrate in a glass moulding press, J. Phys. D. Appl. Phys. 44 (2011), 215302.